UNIVERSITY OF GÄVLE

FACULTY OF ENGINEERING AND SUSTAINABLE DEVELOPMENT
Department of Electrical Engineering, Mathematics and Science

Ocean rogue wave analysis for the development of safer navigation systems

A Thesis submitted to the University of Gävle for the degree of Bachelor of Mathematics

Sergio Manzetti

2023

Student thesis, Basic level (Bachelor degree), 15 HE
Mathematics

Supervisor: Yury Shestopalov
Examiner: Rolf Källström

Contents

Abstract

Rogue waves are unexpectedly high waves of 2.5X the significant wave height and which occur in nearly all phases of nature, from oceans, to fiber-optic cables and atmospheric air-masses. In the ocean, rogue waves pose a significant danger to shipping and fishing vessels and have been found to reach 27.8 meters in height, and attain velocities of up to 100 km/hr. Mechanisms on naval structures for the real-time prediction of rogue waves are currently non-existent, and their development requires a) a good equation for simulating rogue waves and b) a deep study of the wave-trains of rogue waves. In this work, we consider the time-series of four rogue wave trains collected from various sources, including the U.S. Coastal Data Information Program. The method of study encompasses the development piece-wise constant functions from the rogue wave readings by laser/buoys. We use these piece-wise constant functions to form regularized functions as Fourier series, which we consider as weak solutions to the stationary nonlinear Schrödinger equation. The resulting force functions are quantified and compared to physical data of the rogue wave trains. The results show that we obtain a good correlation between the norms of the obtained force functions and the rogue wave height H_{max} and the wave-velocity. The methods developed in the study build a potentially useful foundation for the development of a prediction model in a future study.

1 Introduction

Rogue waves are highly nonlinear phenomena [1] which occur in the worlds oceans [2, 3, 4], on the great lakes [5], in the atmosphere [6] and in fiber optic cables [7]. A rogue wave is normally 2.5X the significant wave height (H_s) and can move up to 100 km/hr [8] potentially inducing devastating damage on ships or at worse capsizing supply and fishing vessels, or breaking apart and sinking giant oil-tankers and cargo ships such as the "MS München", the "MV Derbyshire" and the "El Faro" [9, 10, 11]. There are several mechanisms of formation of rogue waves which encompass the X-interference, Y-interference, wind-to-surface perturbation, perturbation from bottom-morphology and other mechanisms where some are still elusive - such as the rogue wave appearing "out of nowhere and disappearing without a trace" [2]. Several of these mechanisms of formation of rogue waves can be simulated by various approaches accounting for water-depth, wind speed, water temperature, coastal formation and other parameters [2]. Rogue waves can travel at least 1000 km across oceans [2] and merge eventually with the surrounding water via gravity-effects, or collide with land-masses where they vanish.

1.1 Rogue wave modeling

The mathematical function for a rogue wave is known as a soliton, describing a solitary wave which is a self-reinforcing wave-packet that maintains a constant velocity and looses its shape only by gravitational effects [2]. Solitons are the solutions of a widespread class of weakly nonlinear dispersive partial differential equations describing physical systems that can be obtained explicitly using specific initial conditions and boundary conditions. Examples of solitons are waves that have a permanent form and are localized within a region and which can interact with other solitons. Upon collisions, solitons emerge unchanged except for experiencing a phase shift [12]. Solitons are calculated using weakly nonlinear partial differential equations (PDEs) [13, 14, 15, 3, 2], such as the Nonlinear Schrödinger equation, the Korteweg de Vries equation, the MMT equation,

and others [2]. In this section, we shall review the most common differential equations and their soliton-solutions.

1.1.1 The nonlinear Schrödinger equation

The partial differential equations used in modeling rogue waves are intricate and are often equipped with multiple coefficients and non-linear terms. The prime example of such PDEs is the Nonlinear Schrödinger Equation (NLSE) [16] which is the most used for numerical simulations of rogue waves [3, 7, 8, 17, 18, 19]. The NLSE in dimensionless form reads

$$i\psi_t = -\frac{1}{2}\psi_{xx} + \kappa|\psi|^2\psi, \tag{1.1}$$

where ψ is a complex-valued function, κ is the wave-number and i is the imaginary unit. The NLSE can be both inhomogeneous or homogeneous. For the first case, it is first transformed to a homogeneous PDE using specific initial conditions, and subsequently solved using the Darboux-transformation method which ultimately generates n soliton solutions organized in a hierarchical system [3, 7, 19]. The Darboux transformation method is related to the Laplace transformation method and is a mapping between solutions and coefficients of a system of equations of the same form [20]. Let $\psi(x,\lambda), \phi(x,\mu) \in C^2$, where the elements are twice differentiable, and let ψ and ϕ be solutions to the PDE:

$$-\psi_{xx} + u(x)\psi = \lambda\psi, \tag{1.2}$$

where u is a function which yields non-linearity of the following equations

$$\psi_1 = \psi_x + \sigma\psi; \quad \sigma = -\phi_x\phi^{-1} \tag{1.3}$$

which are the solutions to the equation

$$-\psi_{1_{xx}} + u(x)_1\psi_1 = \lambda\psi_1, \tag{1.4}$$

where

$$u_1 = u + 2\sigma_x. \tag{1.5}$$

Here, the forms of ψ_1 and u_1 are given as functions of the solutions and define the Darboux transformation. An example of a soliton function is given by

$$\psi(x,t) = 1 - 4\frac{1+2ix}{1+4t^2+4x^2}e^{ix} \tag{1.6}$$

which was obtained by Dai *et al* [21] as particular solution of the first-order of the hierarchy of solutions of the *variable coefficient inhomogeneous nonlinear Schrödinger equation*(vci-NLSE):

$$i\psi_x + \frac{1}{2}\beta(t)\psi_{tt} + \chi(x)|\psi|^2\psi + \alpha(x)t^2\psi = i\gamma(x)\psi \tag{1.7}$$

where $\alpha(x) = \frac{\beta W_{xx} - \beta_x W_x}{2\beta^2 W}$ (where W is a family of solutions of the form factor specified in [21]) defines the normalized loss rate, the form $\alpha(x)t^2$ accounts for the chirping effects, the parameter $\beta(x) = \beta_0 e^{-\sigma_1 x}$ defines the group-velocity dispersion (i.e., for an entire wave train), while $\chi(x) = \chi_0 e^{\sigma_2 x}$ defines the non-linearity parameters, and $\gamma(x) = \gamma$ defines the loss or gain effects of the wave signal.

The "extended Dysthe equation" (eDe) [22] is a precursor of the NLSE, and is an important PDE to include in this survey of PDEs for rogue waves. The eDe reads

$$\frac{i}{k}\psi_{xyy} + \psi_{yy} + 2ik\psi_x + 2\psi_z = \beta\epsilon^3. \tag{1.8}$$

In order to solve this equation, we first transform [22] the Ede to the NLSE in (1.1) by the procedure given by Dysthe [22] and subsequently obtain the following trial solution (by applying a linear perturbation)

$$\psi = c_0(1+\alpha)e^{1(\theta-\frac{1}{2}ic_0^2t)} \tag{1.9}$$

where α and θ are small real perturbations of the amplitude and phase, respectively [22]. The trial solution in (1.9) is then inserted in (1.1), which is then linearized into a system of two PDEs, with the respective solutions in plane-wave form. These plane-wave solutions contain parameters that satisfy the dispersion relation $\omega^2 = gk$ where k is the wavenumber and g is the acceleration due to gravity [22]. The solutions to the Dysthe equation, as for the general NLSE, are soliton solutions (Peregrine solitons) [23, 24, 25] and are given in the general form.

$$\psi_j(x,t) = (-1)^j + \frac{G_j(x,t) + ixH_j(x,t)}{D_j(x,t)}e^{ix} \tag{1.10}$$

which is shown below with $G = 1, H = 2, D = 1 + 4t^2 + 4x^2$

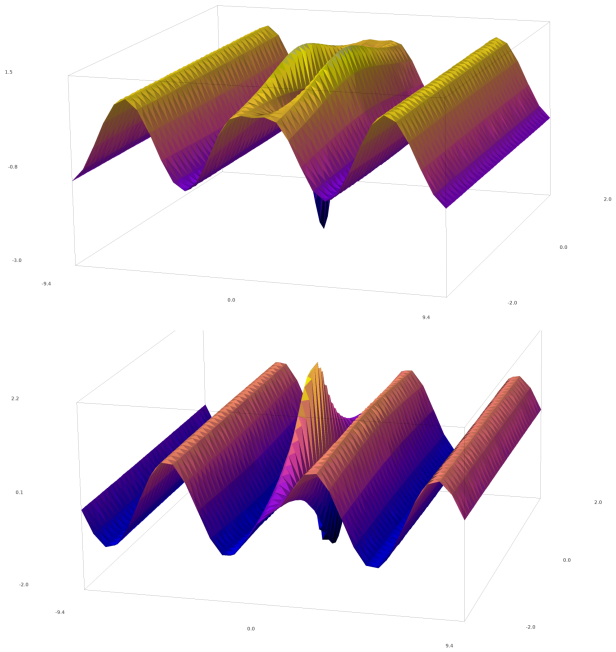

Figure 1. Soliton function in a wave-train. The plot of $\psi_1(x,t)$ from (1.6), generated by the Darboux transformation of the standard NLSE [26]. X-axis: wave-position; Y-axis: time-line;

Z-axis: amplitude. Real and imaginary parts shown respectively above and below. Plotted with SageMATH [27].

1.1.2 Korteweg de Vries equation

The Korteweg de Vries equation is another important equation in the modeling of ocean waves, and is an equation which requires bilinearization into a simplified PDE using the modified Bäcklund transformation technique where one applies the Hirota bilinear operators [28]. The general KdV equation is given by

$$\psi_t + \psi^p \psi_x + \psi_{xxx} = 0 \tag{1.11}$$

where p is a positive parameter. We shall review the results of the specific KdV variant:

$$\psi_t + 6\psi\psi_x + \psi_{xxx} = 0 \tag{1.12}$$

which is subjected to bilinearization [29] using a trial function, also known as steady-state function, which is in principle a soliton function.

$$\psi(x,t) = \left(\frac{p^2}{2}\right)\mathrm{sech}^2\left(\frac{\eta}{2}\right), \tag{1.13}$$

where

$$\eta = px - p^3 t + \eta_0.$$

and p and η are arbitrary constants. This soliton function is shown below in figure 2

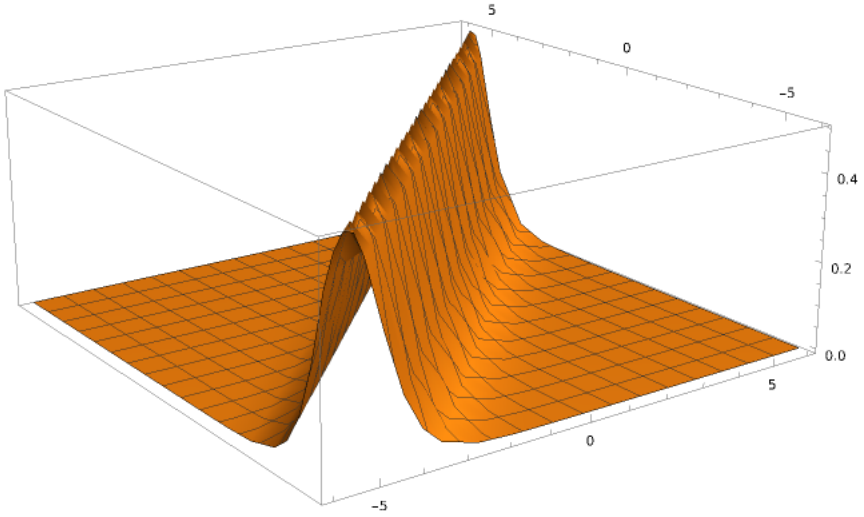

Figure 2. Soliton function. The soliton function used as steady state reference function (1.13) for the bilinearization technique in the modified Bäcklund transformation of the Korteweg de Vries equation. X-axis: wave-position; Y-axis: time-line; Z-axis: amplitude.

The steady-state reference function is written in exponential form $\psi(x,t) = 2p^2(e^{\eta/2} + e^{-\eta/2})$ and is converted to its functional form:

$$\psi(x,t) = 2\frac{\partial^2 \ln[f(x,t)]}{\partial x^2}, \tag{1.14}$$

so that by the bilinearization technique [29] eqn. (1.14) is replaced into the original KdV Equation (1.12) and integrated with respect to x to give:

$$f_{xt}f - f_x f_t + f_{xxxx}f - 4f_{xxx}f_x + 3(f_{xx})^2 = 0 \tag{1.15}$$

which is the bilinearized variant of the Korteweg–de Vries Equation (1.12) obtained from the bilinearization using Bäcklund transformation method [29]. It is at this stage that the simplicity of the transformed form of the KdV equation in (1.15) becomes evident, where the operators are replaced by the Hirota operators [28] and yield the simple PDE:

$$D_x(D_t + D_x^3)f \cdot f = 0, \tag{1.16}$$

which has the general solution given by:

$$\Psi = 1 + \epsilon(e^{\eta_1} + e^{\eta_2}) - \epsilon^2 \frac{F(\Omega_1 - \Omega_2, p_1 - p_2)}{F(\Omega_1 + \Omega_2, p_1 + p_2)} e^{\eta_1 + \eta_2} \tag{1.17}$$

where η_1 and η_2 are the functions with the independent variables x and t as given in the steady-state function in (1.13) for each of the solitons. $\Omega_1 = -p_1^3$ and $\Omega_2 = -p_2^3$, following the same definition for (1.13) for each soliton. η represents the perturbations [29]. A particular solution of (1.16) is given by :

$$\Psi = e^{2it} \frac{\cos(2\sqrt{x})\mathrm{sech}(2\sqrt{x}) + i\sqrt{2}\tanh(2t)}{\sqrt{2} - \cos(2\sqrt{x})\mathrm{sech}(2\sqrt{x})}, \tag{1.18}$$

which is plotted below in Fig 3. Interestingly, the KdW equation has also been solved using a nonlinear Fourier method [30, 31], which is represented by a superposition of nonlinear oscillatory modes of the wave spectrum. This equation, developed by Osborne [30, 31], has the capacity to include a large number of non-linear oscillatory patterns, also known as multi-quasi-cnoidal waves, which are used to form the rogue wave by superposition in constructive phases. These solutions to the original KdV Equation (1.12) include several solitons, depending on the number of degrees of freedom selected for the numerical simulation of the KdV equation. This yields a 3D wave as a complex function composed of multiple solitons and radiation components in the simulated wave train [30] (Fig. 3).

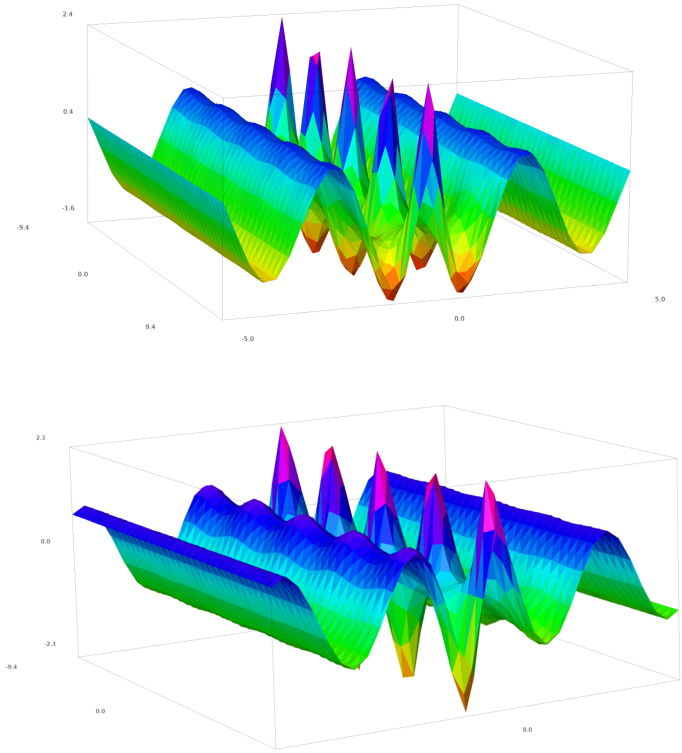

Figure 3. Soliton solution of the Korteweg de Vries equation. The function of this plot is given in (1.18). X-axis: wave-position; Y-axis: time-line; Z-axis: amplitude. Real and imaginary parts shown respectively above and below. The solution is developed using a nonlinear Fourier method which is not discussed in detail here, but can be found in the reference sources [30, 31].

1.1.3 The MMT equation

The MMT equation is a one-dimensional nonlinear equation, which was originally proposed by Majda, McLaughlin and Tabak [32]. The MMT equation gives soliton-like solutions, which have been analyzed in detail by Zhakarov [33, 34, 35], and gives four-wave resonant interaction between waves (where bichromatic mother waves are generated to give birth to a daughter wave), which, when coupled with large-scale forces and small-scale damping, yields a family of waves that exhibit direct and inverse cascades [36]. This

family of waves is modeled by the MMT equation:

$$i\psi_t = |\partial_x|^\alpha \psi + |\partial_x|^{-\beta/4}\left(\left||\partial_x|^{-\beta/4}\psi|^2\right| \cdot |\partial_x|^{-\beta/4}\psi\right) \tag{1.19}$$

here $|\partial_x|^\alpha$ is the pseudo-differential operator defined on the real axis through the Fourier transform:

$$|\partial_x|^\alpha \psi(k) = |k|^\alpha \hat{\psi}(k). \tag{1.20}$$

Equation (1.19) is a Hamiltonian system with the Hamiltonian operator:

$$H = \int \left(\left| |\partial_x|^{\alpha/2}\psi \right|^2 + \frac{1}{2}\left| |\partial_x|^{-\beta/4}\psi \right|^4 \right) \mathrm{d}x \tag{1.21}$$

where the parameter α determines the dispersion relation:

$$\omega = \Omega(k) = |k|^\alpha. \tag{1.22}$$

The given MMT equation is in principle an extension of the NLSE, as the usual NLSE results by putting $\alpha = 2$ [32]. When $\alpha = 1/2$ however, the equation describes the water wave dispersion law with $\omega = \sqrt{|k|}$. Furthermore, when $\alpha \geq 1$ the dispersion relation is convex, which otherwise does not hold when $\alpha < 1$. The convex property of the dispersion relation gives a crescent behaviour of the attenuating waves, leading to the formation of a rogue wave. The parameter β is the nonlinear term, when $\beta = 0$ we have a standard cubic power law, and when β grows, the nonlinearity becomes weaker because of nonlocal smoothing in the variable x [32]. Majda et al [32] introduces the conserved norm in the MMT equation:

$$|\psi|^2 = \int_{\mathbb{R}} |\psi|^2 dx \tag{1.23}$$

and the conserved linear momentum by the time-evolution of equation (1.19):

$$P = \int_{\mathbb{R}} |\psi\hat{\psi}_x - \psi_x\hat{\psi}| dx \tag{1.24}$$

Furthermore, one transform the MMT prior to numerical simulation to a Fourier-space form, which is given in [32]. This is particularly convenient when studying the energy-transfer mechanism from waves surrounding the rogue wave. The numerical study of the MMT equation done by [32] uses a trial function given in the form:

$$\psi(x,t) = \epsilon\left[\sum_{j=1}^{4} A_j(T)e^{i[(]k_j x - \Omega(k_j)t]} + \epsilon^2\hat{\psi}(x,t)\right] \tag{1.25}$$

where $\Omega(k)$ denotes the dispersion relation while the slow-time is given by $T = \epsilon^2 t$. An example of the MMT-trial function is

$$\psi(x,t) = 4(e^{i(-3t+3x)} + 0.04e^{ix}t^2), \tag{1.26}$$

which is plotted below.

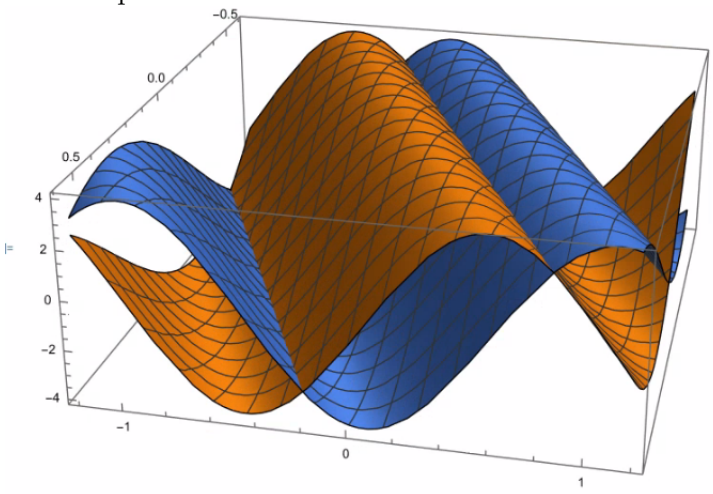

Figure 3. General form of the trial function for the MMT equation. The function of this plot is given in (1.26). X-axis: wave-position; Y-axis: time-line; Z-axis: amplitude. Real and imaginary parts shown respectively in blue and orange.

Insertion of (1.25) in (1.19) produces a rather elaborate differential equation for $\hat{\psi}$ given in [32], which corresponds to a forced linear oscillator, with a secular growth in time. Under specific conditions given in [32], the resulting equation is simplified into a system

of ODEs. If specific resonance conditions are met, then the ODEs give a maximal energy interchange between wave-modes, which gives an estimate of the transfer of energy which yield eventually a resonance quartet, which exist only for non-convex dispersion laws. Additional equations for rogue wave modeling are the one-dimensional nonlinear dispersive wave equations [36, 37, 37], the Hirota equation [28], the parity- and time-symmetric ($\mathcal{PT}$-symmetric) nonlocal equation [38, 39, 40] and as briefly mentioned before, the Osborne equations developed by Fourier analysis [30, 31], which are all thoroughly described in [2].

2 Wave-reading analysis using piece-wise constant functions

In this section, we shall introduce the notions of this study. The main motivation of this study is to analyse laser/buoy readings of rogue wave-trains from the ocean so we can identify conserved patterns of rogue-wave formation and possibly some warning signals. An example of such laser/buoy readings is given below in Figure 4. Wave-readings are laser/buoys registrations of the amplitudes of wave-trains with respect to time, hence, wave-readings are in practice time-series of waves that can be defined as:

Definition 2.1. The set of amplitudes of rogue waves. The set of amplitudes from a laser/buoy reading of rogue wave is defined by a finite sequence of coordinates $r_n \in \mathbb{R}^2$, given by $r_n = \{(\xi_1, \eta_1), (\xi_2, \eta_2), \cdots, (\xi_n, \eta_n)\}$, where n denotes the number of coordinates.

Such wave-readings are outputs from data-registration in the ocean, using bouys or lasers under oil-rigs, which measure the stability and level of the rig over the sea (given depressions in the sea-bed given extraction of oil/gas). An example is shown below, where the a time-series of wave at the buoy at Aunuu of American Samoa is shown.

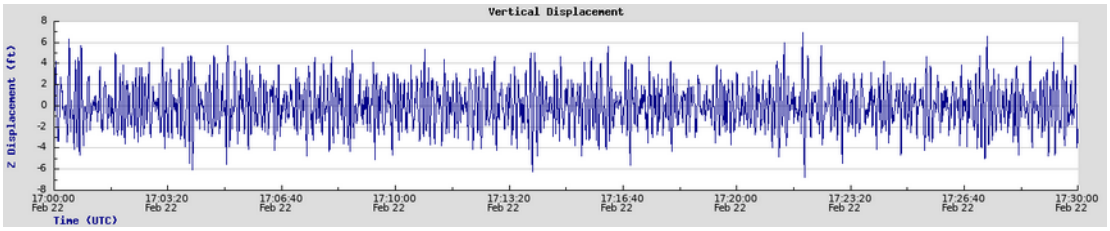

Figure 4. Wave-reading example. The figure shows the wave-train registered with a buoy of the US Coastal Data Information Program located at American Samoa (https://cdip.ucsd.edu/).

Wave-readings reproduce the wave-patterns of a wave-train perturbed under various weather conditions, which can give rise to the formation of wave-packets. Wavepackets are groups of localized waves that travel as a unit and can be measured precisely in such wave-readings from the ocean. Wavepackets are conventionally represented by plane-wave functions of the form:

$$u(x,t) = e^{i(\mathbf{k}x-\omega t)}, \tag{2.1}$$

which satisfy the wave-equation:

$$u_{tt} = \alpha u_{xx}, \tag{2.2}$$

which can be solved either by developing the Fourier coefficients or using d'Alembert's formula, provided intial and boundary conditions. During ocean storms, such wavepackets can display extreme velocities and monstrous wave-heights, with registered velocities reaching up to 100 km/hr for individual crests with height 27.8m, contained in a wavepacket extending more than 1 km in length [8]. The wave-reading from the related buoy in the Atlantic ocean is shown below in Figure 5 and is an ideal example of the basis of forming piece-wise constant functions.

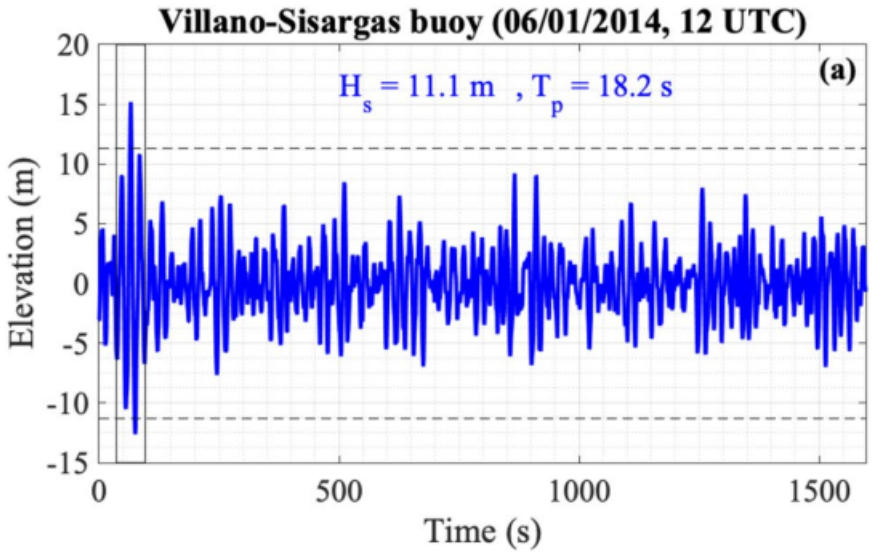

Figure 5. Rogue wave-packets formed in ocean waves. The figure displays a wave-reading of the time-series of a rogue-wave train, where the rogue wave appears inside a wave-packet localized to the out-most left part of the plot, from 0-100 seconds. This wave-packet travelled at a velocity of 100 km /hr. Adapted with permissions from [8]. Copyright Nature Scientific publishing.

2.0.1 Piece-wise constant functions and their Fourier series

We shall now introduce the notions required to develop a study of the rogue-wave readings. An indicator function, defined on $A_j = [\xi_{j-1}, \xi_j] \subset [-a, a]$ is defined by

$$\chi_{A_j}(\xi) = \begin{cases} 1 & if \quad \xi \in A_j \\ 0 & if \quad \xi \notin A_j. \end{cases} \tag{2.3}$$

A piece-wise constant function is of the form

$$f(\xi) := \sum_{i=1}^{n} \eta_j \chi_{A_j}(\xi). \tag{2.4}$$

We define a partitioning on the interval $[-a, a]$ to be a set of interval $P = \{A_1, A_2, \cdots, A_n\}$ such that $[-a, a] = \cup_{j=1}^{n} A_j$ and $A_i \cap A_j$ is either empty or vanish at most at a single point where $i \neq j$. We then say that $\{A_1, \cdots, A_n\}$ is an almost disjoint partitioning of $[-a, a]$. Let $\mathscr{S}([-a, a])$ be the set of all piece-wise constant functions on $[-a, a]$ and let $\mathscr{S}_P([-a, a])$ be the subset of such functions that are constant on every interval A_j ($\bigcup_{j=0}^{n-1} \xi_i, \xi_{j+1} = [-a, a]$), such that $\mathscr{S}_P \subset \mathscr{S}$. A partition P can be refined, by forming a new almost disjoint union of its sub-intervals. This refinement can be applied to any simple indicator function or to a sum of indicator functions. Moreover, given two partitions $P = \{A_1, \cdots, A_n\}$ and $Q = \{B_1, \cdots, B_n\}$ there exists a common refinement $R = \{C_1, \cdots, C_n\}$ so that each A_i and B_j is an almost disjoint union of sets from C. It follows that $\mathscr{S}_P([-a, a]) \subseteq \mathscr{S}_R([-a, a])$, $\mathscr{S}_Q \subseteq \mathscr{S}_R$. Therefore, if $f \in \mathscr{S}_p([-a, a])$, $g \in \mathscr{S}_Q$ it is clear that $\alpha f + \beta g \in \mathscr{S}_R([-a, a])$, where $\alpha,\ \beta \in \mathbb{R}$. We exemplify such a refinement in figure 6. Such a described piece-wise constant function is constructed for each wave-reading (see Fig. 5 of examples of such wave-readings). First, we introduce two examples of piece-wise constant functions, which are also simple functions composed of a finite linear combination of indicator functions. These two examples are introduced for respectively a uniform grid (composed of n partitions of equal length) and a non-uniform grid (composed of n partitions of unequal length).

Example 2.0.1. Here we show an example of a piece-wise constant function $f(t)$ on a *uniform* grid and an example of piece-wise constant function $g(t)$ on a *non-uniform* grid on the vector space $\mathscr{S}[-3, 3]$ characterized by the points $\xi_j,\ j = 0, 1, 2, \cdots, n$ and with $n = 4$

$$f(\xi) := \sum_{j=1}^{4} \eta_j \chi_{A_j}(\xi), \tag{2.5}$$

where A_j=$[\xi_{j-1}, \xi_j]$, $\xi_0 = -2,\ \xi_1 = -1,\ \xi_2 = 0,\ \xi_3 = 1, \xi_4 = 2,$

$$f(\xi) = \begin{cases} 2, & -2 \leq \xi < -1 \\ 1, & -1 \leq \xi < 0 \\ 2, & 0 \leq \xi < 1 \\ 3, & 1 \leq \xi \leq 2, \end{cases} \tag{2.6}$$

and with $n = 4$

$$g(\xi) := \sum_{j=1}^{4} \eta_j \chi_{A_j}(\xi), \tag{2.7}$$

where A_j=$[\xi_{j-1}, \xi_j]$, where $\xi_0 = -3,\ \xi_1 = -\frac{3}{2},\ \xi_2 = \frac{1}{5}, \xi_3 = 1, \xi_4 = 2$

$$g(\xi) = \begin{cases} 2, & -3 \leq \xi < -\frac{3}{2} \\ 1, & -\frac{3}{2} \leq \xi < \frac{1}{5} \\ 3, & 0.2 \leq \xi < 1 \\ 6, & 1 \leq \xi \leq 3 \end{cases} \tag{2.8}$$

which are plotted jointly in (Fig. 6).

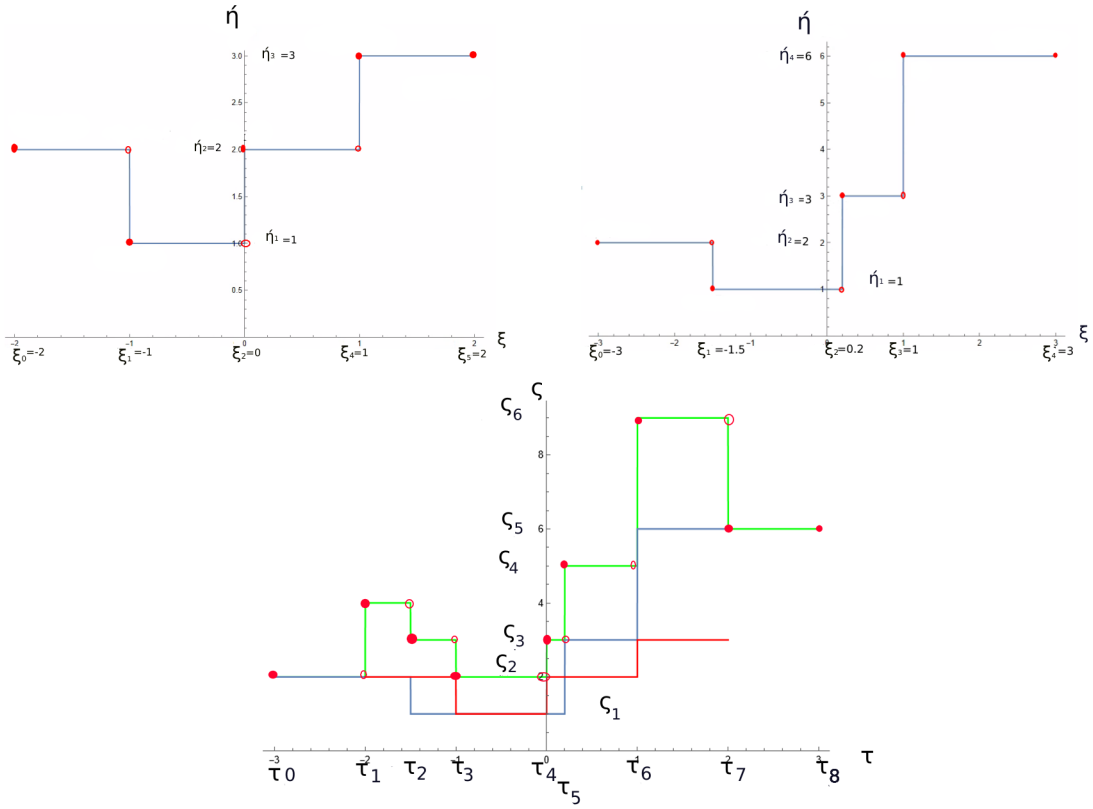

Figure 6. The piece-wise constant function. From top left to bottom, $f, g, h = f + g$. Circled and pointed in red are the coordinates of the intervals for the stepwise function given in (2.6) on the interval $[-2, 2]$. Respective ξ^f-values: $\xi_0 = -2,\ \xi_1 = -1,\ \xi_2 = 0,\ \xi_3 = 1, \xi_4 = 2$. Respective η^f-values: $\eta_1 = 2,\ \eta_2 = 1,\ \eta_3 = 2, \eta_4 = 3$. Respective ξ^g-values: $\xi_0 = -3,\ \xi_1 = -1.5,\ \xi_2 = 0.2, \xi_3 = 1, \xi_4 = 2$. Respective η^g-values: $\eta_1 = 2,\ \eta_2 = 1,\ \eta_3 = 3,\ \eta_4 = 6$. Bottom: h: green color; f: red color; g: blue color. Note that the lowermost picture shows the τ^h values on the x-axis and ς^h on the y-axis, which are not-related to neither the ξ^g or ξ^g values on the upper plots. The bottom picture shows that h yields a refinement of $\mathscr{S}$ into $n{=}8$ partitions, while $\mathscr{S}$ is subdivided into n=4 partitions for f and g. The relationship between the partitions is thence given by $f, g \in \mathscr{S}_P \subset \mathscr{S}$ while $h \in \mathscr{S}_{P_P} \subset \mathscr{S}_P \subset \mathscr{S}$.

2.0.2 The Fourier series of the piece-wise constant function on a uniform grid.

The Fourier series of the indicator function $\chi_{A_j}(t)$ can be calculated by the formula:

$$\chi_{A_j}(t) := \alpha_0^j + \sum_{k=1}^{\infty} \alpha_k^j \cos \omega k t + \beta_k^j \sin \omega k t \tag{2.9}$$

where $\omega = \frac{\pi}{a}$ and which converges to $\chi_{A_j}(t)$ point-wise at every $t \in [-a, a]$, except for discontinuity points. The Fourier coefficients can be computed as:

$$\alpha_0^j = \frac{1}{2a} \int_{-a}^{a} \chi_{A_j}(t) \mathrm{d}t = \frac{1}{2a}(\xi_j - \xi_{j-1}) = \frac{h_j}{2a}, \tag{2.10}$$

where $h_j = \xi_j - \xi_{j-1}$. Then, let $h = \frac{2a}{n}$ and we obtain

$$\alpha_0 = \frac{h}{2a} = \frac{1}{n} \tag{2.11}$$

Now we calculate α_k^j:

$$\begin{aligned} &\alpha_k^j = \frac{1}{a} \int_{-a}^{a} \chi_{A_j}(t) \cos \omega k t \mathrm{d}t = \frac{1}{a} \int_{\xi_{j-1}}^{\xi_j} \cos \omega k t \mathrm{d}t = \\ &\frac{1}{\pi k} \left[\sin \frac{\pi k \xi_j}{h} - \sin \frac{\pi k \xi_{j-1}}{h} \right] = \frac{2}{\pi k} \sin \left(\omega k \frac{h_j}{2} \right) \cos \left(\omega k \frac{\xi_j + \xi_{j-1}}{2} \right), \end{aligned} \tag{2.12}$$

where we made use of the trigonometric identity: $\sin x - \sin y = 2 \sin \frac{x-y}{2} \cos \frac{x+y}{2}$. Now, let $\xi_j = -a + jh$, $j = 0, 1, \cdots, n$. Also, let $h_j = h = \frac{2a}{n}$ and $\xi_j + \xi_{j-1} = -2a + (2j-1)h$. Then we obtain for the cosine term brackets: $\omega k \frac{(\xi_j + \xi_{j-1})}{2} = -\pi k + (2j-1)\frac{\pi k}{n}$ such that

$$\alpha_k^j = \frac{2(-1)^k}{\pi k} \sin \left(\omega k \frac{h_j}{2} \right) \cos \big((2j-1) \frac{\pi k}{n} \big), \tag{2.13}$$

where with $h_j = \xi_j - \xi_{j-1}$ and $w_k = \frac{\pi k}{n}$ obtain:

$$\alpha_k^j = 2 \frac{(-1)^k}{\pi k} \sin w_k \cos \big(w_k (2j-1) \big) \tag{2.14}$$

The same is done for β_k^j:

$$\beta_k^j = \frac{1}{a}\int_{-a}^{a} \chi_{A_j}(t)\sin(\omega k t)\mathrm{d}t = \frac{1}{a}\int_{\xi_{j-1}}^{\xi_j} \sin\omega k t \mathrm{d}t = \\ \frac{1}{\pi k}\left[\cos\frac{\pi k \xi_{j-1}}{h} - \cos\frac{\pi k \xi_j}{h}\right] = \frac{2}{\pi k}\sin\left(\omega k\frac{h_j}{2}\right)\sin\left(\omega k\frac{\xi_j+\xi_{j-1}}{2}\right), \tag{2.15}$$

Again, with $\xi_j = -a+jh$, $j = 0, 1, \cdots, n$, $h_j = h = \frac{2a}{n}$ with $\xi_j+\xi_{j-1} = -2a+(2j-1)h$ we obtain for the second sine term on the RHS (using the trigonometric identity $\sin(a+b) = \cos(b)\sin(a) + \cos(a)\sin(b)$:

$$\sin\omega k\frac{\xi_j+\xi_{j-1}}{2} = \sin\left(-\pi k + (2j-1)\frac{\pi k}{n}\right) = (-1)^k \sin\big((2j-1)\frac{\pi k}{n}\big), \tag{2.16}$$

which we then rewrite with $w_k = \frac{\pi k}{n}$ and $h_j = \xi_j - \xi_{j-1}$ to:

$$\beta_k = \frac{2(-1)^k}{\pi k}\sin w_k \sin\big(w_k(2j-1)\big). \tag{2.17}$$

From this we obtain the Fourier series for the piece-wise constant function.

$$f_n(t) = \sum_{j=1}^{n} \eta_j \chi_{A_j}(t), \tag{2.18}$$

where the uniform grid is given by

$$h_j = h, \quad j = 1, 2, \cdots, n \\ \xi_j = -a + jh, \quad j = 0, 1, \cdots, n, \quad h = \tfrac{2a}{n}, \tag{2.19}$$

and we obtain

$$\alpha_0 = \frac{h}{2a}\sum_{j=1}^{n}\eta_j = \frac{1}{n}\sum_{j=1}^{n}\eta_j; \tag{2.20}$$

$$\alpha_k = \frac{2(-1)^k}{\pi k}\sin w_k \sum_{j=1}^{n}\eta_j \cos\big((2j-1)w_k\big); \tag{2.21}$$

$$\beta_k = \frac{2(-1)^k}{\pi k}\sin w_k \sum_{j=1}^{n}\eta_j \sin\big((2j-1)w_k\big), \tag{2.22}$$

where $w_k = \frac{\pi k}{n}$ and $k = 1, 2, \cdots, n$.

2.0.3 The Fourier series for a piece-wise-constant function on a non-uniform grid.

Since the piece-wise constant function on a non-uniform grid supported on $[-a, a] = \cup_{j=1}^{n} A_j = \cup_{j=1}^{n} [\xi_{j-1}, \xi_j],\ -a = \xi_0,\ a = \xi_n$ is given by:

$$f_n(t) = \sum_{j=1}^{n} \eta_j \chi_{A_j}(t), \tag{2.23}$$

and the Fourier series is given by:

$$f_n(t) = \alpha_0 + \sum_{k=1}^{\infty} \alpha_k \cos(\omega k t) + \beta_k \sin(\omega k t), \tag{2.24}$$

where, by $\omega = \frac{\pi}{a}$ we obtain the coefficients on the non-uniform grid:

$$\alpha_0 = \frac{1}{2a} \int_{-a}^{a} f_n(t) \mathrm{d}t = \frac{1}{2a} \sum_{j=1}^{n} \eta_j (\xi_j - \xi_{j-1}) \tag{2.25}$$

$$\alpha_k = \frac{1}{a} \int_{-a}^{a} f_n(t) \cos(\omega k t) \mathrm{d}t = \frac{2}{\pi k} \sum_{j=1}^{n} \eta_j \sin\left(\omega k \frac{h_j}{2}\right) \cos\left(\omega k \frac{\xi_j + \xi_{j-1}}{2}\right) \tag{2.26}$$

$$\beta_k = \frac{1}{a} \int_{-a}^{a} f_n(t) \sin(\omega k t) \mathrm{d}t = \frac{2}{\pi k} \sum_{j=1}^{n} \eta_j \sin\left(\omega k \frac{h_j}{2}\right) \sin\left(\omega k \frac{\xi_j + \xi_{j-1}}{2}\right) \tag{2.27}$$

We prove two lemmas showing the essential properties of stepwise functions.

2.0.4 Two lemmas for the Fourier series

Lemma 2.1. *Let $f \in \mathscr{S}_P[-a, a]$ where the partitioning P is uniform. Then, the Fourier coefficients of f are independent of a.*

Proof. Let the indicator function $\chi_{A_j}(t)$ be

$$\chi_{A_j}(t) = \begin{cases} 1, & \xi_{j-1} < t < \xi_j \\ 0, & \text{elsewhere,} \end{cases} \tag{2.28}$$

The function f is of the form $f(t) = \sum \eta_j \chi_{A_j}(t)$.

Let us calculate the Fourier coefficients of the Fourier series over $[-a, a]$ with an arbitrary a of the indicator function of interval $A_j = \xi_{j-1} < t < \xi_j$:

$$\alpha_0^j = \frac{1}{2a} \int_{-a}^{a} \chi_{A_j}(t) \mathrm{d}t = \frac{1}{2a} \int_{\xi_j - 1}^{\xi_j} \mathrm{d}t = \frac{1}{2a}(\xi_j - \xi_{j-1}) \tag{2.29}$$

with $(\xi_j - \xi_{j-1}) = h$ we get:

$$\alpha_0^j = \frac{h}{2a} \tag{2.30}$$

Finally, since $h = \frac{2a}{n}$ we get:

$$\alpha_0^j = \frac{1}{n}, \tag{2.31}$$

which is independent of a. Concomitantly, for the step-wise function we get:

$$\alpha_0 = \frac{1}{2a} \int_{-a}^{a} f_n(t) \mathrm{d}t = \sum_{j=1}^{n} \eta_j \alpha_0^j = \frac{1}{2a} \sum_{j=1}^{n} \eta_j h_j = \frac{1}{2a} \sum_{j=1}^{n} \eta_j (\xi_j - \xi_{j-1}), \tag{2.32}$$

since $(\xi_j - \xi_{j-1}) = h_j$ is constant, we can form the integral as:

$$\frac{h_j}{2a} \sum_{j=1}^{n} \eta_j, \tag{2.33}$$

and with $h_j = \frac{2a}{n}$, we readily obtain

$$\alpha_0 = \frac{1}{n} \sum_{j=1}^{n} \eta_j. \tag{2.34}$$

Now, with α_k and β_k as calculated in the previous section:

$$\alpha_k = \frac{2}{\pi k}\sum_{j=1}^{n}\eta_j \sin\left(\omega k\frac{h_j}{2}\right)\cos\left(\omega k\frac{\xi_j+\xi_{j-1}}{2}\right) \tag{2.35}$$

and

$$\beta_k = \frac{2}{\pi k}\sum_{j=1}^{n}\eta_j \sin\left(\omega k\frac{h_j}{2}\right)\sin\left(\omega k\frac{\xi_j+\xi_{j-1}}{2}\right), \tag{2.36}$$

we express f as a Fourier series:

$$\begin{aligned}\sum_{j=1}^{n}\eta_j\chi_{A_j}(t) = \frac{1}{n}\sum_{j=1}^{n}\eta_j + \sum_{k=1}^{\infty}\left[\frac{2(-1)^k}{\pi k}\sin w_k\sum_{j=1}^{n}\eta_j\cos\big((2j-1)w_k\big)\right]\cos\omega kt + \\ \left[\frac{2(-1)^k}{\pi k}\sin w_k\sum_{j=1}^{n}\eta_j\sin\big((2j-1)w_k\big)\right]\sin\omega kt,\end{aligned} \tag{2.37}$$

where $\omega = \frac{\pi}{a}$ on $[-a,a]$. Herein, we have therefore shown that each Fourier coefficient does not depend on a and we can therefore formulate $f_n(t)$ as a Fourier series independent of a. Calculations for α_k and β_k are given in 7.1. □

Lemma 2.2. *Given the n first Fourier coefficients of a function $f \in \mathscr{S}$ (sine or cosine):*

$$\begin{aligned}&\{\alpha_0, \alpha_1, \cdots, \alpha_{n-1}\}, \textit{ or,}\\ &\{\beta_1, \beta_2, \cdots, \beta_n\}\end{aligned} \tag{2.38}$$

one can uniquely determine the stepwise function (numbers η_j, $j = 1, 2, \cdots n$) on a given grid of points, ξ_j, $j = 0, 1, \cdots n$, provided that the system of linear equations of n-first Fourier coefficients and n-first Fourier integrals is represented by a square matrix B_n which is composed of the entries $B_n = (b_{kj})$ where $k = 1, 2, \cdots, n$ is the number (and index) of rows and $j = 1, 2, \cdots, n$ is the number (and index) of columns, and that $|B_n| \neq 0$. Hence, the matrix must be invertible.

Proof. Consider the α_k coefficient in the system of linear equations:

$$B_n \begin{pmatrix} \eta_1 \\ \eta_2 \\ \vdots \\ \eta_n \end{pmatrix} = \begin{pmatrix} \alpha_0^1(f) \\ \alpha_1^2(f) \\ \vdots \\ \alpha_{n-1}^n(f) \end{pmatrix}, \tag{2.39}$$

where, α_k with $k = 0, 1, \cdots, n$ for each successive row. Then we can form the matrix of coefficients by

$$B_n = \begin{pmatrix} \alpha_0^1(A_1) & \alpha_0^2(A_2) & \cdots & \alpha_0^n(A_n) \\ \alpha_1^1(A_1) & \alpha_1^2(A_2) & \cdots & \alpha_1^n(A_n) \\ \vdots & \vdots & \vdots & \vdots \\ \alpha_{n-1}^1(A_1) & \alpha_{n-1}^2(A_2) & \cdots & \alpha_{n-1}^n(A_n) \end{pmatrix}, \tag{2.40}$$

where $B_n = (b_{k,j})_{0 \le k,j \le n}$ and where $A_1, A_2, \cdots A_n$ are the n intervals of a piece-wise constant function. We claim that we can obtain η_j from α_k^j using (2.39), provided that B_n is invertible ($|B_n| \neq 0$) and that k is an odd-numbered integer (given the resulting zeros of the sine function for even k values in w_k in α_k^j).

Therefore for B_n we obtain with $\alpha_k^j = 2\frac{(-1)^k}{\pi k} \sin w_k \cos\big(w_k(2j-1)\big)$, where $w_k = \frac{\pi k}{n}$ and with $\alpha_0 = \frac{1}{n}$:

$$B_n = \begin{pmatrix} \frac{1}{1} & \cdots & \frac{1}{n} \\ 2\frac{(-1)^2}{\pi} \sin w_1 \cos\big(w_1(2-1)\big) & \cdots & 2\frac{(-1)^2}{\pi} \sin w_1 \cos\big(w_1(2(n)-1)\big) \\ \vdots & \vdots\vdots\vdots & \vdots \\ 2\frac{(-1)^{n-1}}{\pi(n-1))} \sin w_{n-1} \cos\big(w_{n-1}(2-1)\big) & \cdots & 2\frac{(-1)^{n-1}}{\pi(n-1))} \sin w_{n-1} \cos\big(w_{n-1}(2(n)-1)\big) \end{pmatrix}, \tag{2.41}$$

where $B_n = (b_{k,j})_{0 \le k,j \le n}$. By B_n we can identify η_j in (2.39) provided $|B_n| \neq 0$.

Take the following series for $k = 3, 5, 7, 9$ and obtain:

$$B_4 = \begin{pmatrix} -\frac{3}{\pi} & \frac{3}{\pi} & \frac{3}{\pi} & -\frac{3}{\pi} \\ \frac{5}{\pi} & -\frac{5}{\pi} & -\frac{5}{\pi} & \frac{5}{\pi} \\ -\frac{7}{\pi} & \frac{7}{\pi} & \frac{7}{\pi} & -\frac{7}{\pi} \\ \frac{9}{\pi} & -\frac{9}{\pi} & -\frac{9}{\pi} & \frac{9}{\pi} \end{pmatrix} \tag{2.42}$$

which gives:

$$\begin{pmatrix} \eta_1 \\ \eta_2 \\ \eta_3 \\ \eta_4 \end{pmatrix} \begin{pmatrix} -\frac{3}{\pi} & \frac{3}{\pi} & \frac{3}{\pi} & -\frac{3}{\pi} \\ \frac{5}{\pi} & -\frac{5}{\pi} & -\frac{5}{\pi} & \frac{5}{\pi} \\ -\frac{7}{\pi} & \frac{7}{\pi} & \frac{7}{\pi} & -\frac{7}{\pi} \\ \frac{9}{\pi} & -\frac{9}{\pi} & -\frac{9}{\pi} & \frac{9}{\pi} \end{pmatrix} = \begin{pmatrix} 2 \\ 1 \\ 2 \\ 3 \end{pmatrix} \begin{pmatrix} -\frac{3}{\pi} & \frac{3}{\pi} & \frac{3}{\pi} & -\frac{3}{\pi} \\ \frac{5}{\pi} & -\frac{5}{\pi} & -\frac{5}{\pi} & \frac{5}{\pi} \\ -\frac{7}{\pi} & \frac{7}{\pi} & \frac{7}{\pi} & -\frac{7}{\pi} \\ \frac{9}{\pi} & -\frac{9}{\pi} & -\frac{9}{\pi} & \frac{9}{\pi} \end{pmatrix} \tag{2.43}$$

which gives:

$$\begin{pmatrix} \eta_1 \\ \eta_2 \\ \eta_3 \\ \eta_4 \end{pmatrix} = \begin{pmatrix} 2 \\ 1 \\ 2 \\ 3 \end{pmatrix} \tag{2.44}$$

□

2.0.5 Examples of calculations of Fourier coefficients and Fourier series.

In this section we shall return to the examples of the piece-wise constant functions given in (2.6) and (2.8) and calculate their respective Fourier coefficients and Fourier series.

Example 2.0.2. For the piece-wise constant function

$$f(\xi) := \sum_{j=1}^{4} \eta_j \chi_{A_j}(\xi), \tag{2.45}$$

where $j = 1, 2, 3, 4, 5$ and A_j=$[\xi_{j-1}, \xi_j]$, and $\xi_0 = -2,\ \xi_1 = -1,\ \xi_2 = 0,\ \xi_3 = 1, \xi_4 = 2$ and $\eta_j = [\eta_1, \eta_2, \eta_1, \eta_3] = [2, 1, 2, 3]$

$$f(\xi) = \begin{cases} 2, & -2 \le \xi < -1 \\ 1, & -1 \le \xi < 0 \\ 2, & 0 \le \xi < 1 \\ 3, & 1 \le \xi \le 2 \end{cases} \tag{2.46}$$

The Fourier coefficients are:

$$\alpha_0 = \frac{1}{2\pi}\int_{-\pi}^{\pi} f(\xi) = \frac{1}{2\pi}\left(\int_{-\pi}^{-\pi/2} 2\mathrm{d}\xi + \int_{-\pi/2}^{0} 1\mathrm{d}\xi + \int_{0}^{\pi/2} 2\mathrm{d}\xi + \int_{\pi/2}^{\pi} 3\mathrm{d}\xi\right) = 2 \tag{2.47}$$

and α_k, with $j = 1, 2, \cdots, n$ is given by:

$$\begin{aligned}
\alpha_k^j &= \frac{\eta_j(-1)^k}{\pi k}\sin\frac{\pi k}{n}\cos(2j-1)\frac{\pi k}{n} \\
\alpha_k^1 &= \frac{2(-1)^k}{\pi k}\sin\frac{\pi k}{4}\cos\frac{\pi k}{4} \\
\alpha_k^2 &= \frac{(-1)^k}{\pi k}\sin\frac{\pi k}{4}\cos\frac{3\pi k}{4} \\
\alpha_k^3 &= \frac{2(-1)^k}{\pi k}\sin\frac{\pi k}{4}\cos\frac{5\pi k}{4} \\
\alpha_k^4 &= \frac{3(-1)^k}{\pi k}\sin\frac{\pi k}{4}\cos\frac{7\pi k}{4} \\
\alpha_k &= \sum_{j=1}^{4}\alpha_k^j = \frac{(-1)^k}{\pi k}\sin\frac{\pi k}{4}\left(2\cos\frac{\pi k}{4} + \cos\frac{3\pi k}{4} + 2\cos\frac{5\pi k}{4} + 3\cos\frac{7\pi k}{4}\right)
\end{aligned} \tag{2.48}$$

and

$$\begin{aligned}
\beta_k^j &= \frac{\eta_j(-1)^k}{\pi k}\sin\frac{\pi k}{n}\sin(2j-1)\frac{\pi k}{n} \\
\beta_k^1 &= \frac{2(-1)^k}{\pi k}\sin\frac{\pi k}{4}\sin\frac{\pi k}{4} \\
\beta_k^2 &= \frac{(-1)^k}{\pi k}\sin\frac{\pi k}{4}\sin\frac{3\pi k}{4} \\
\beta_k^3 &= \frac{2(-1)^k}{\pi k}\sin\frac{\pi k}{4}\sin\frac{5\pi k}{4} \\
\beta_k^4 &= \frac{3(-1)^k}{\pi k}\sin\frac{\pi k}{4}\sin\frac{7\pi k}{4} \\
\beta_k &= \sum_{j=1}^{4}\beta_k^j = \frac{(-1)^k}{\pi k}\sin\frac{\pi k}{4}\left(2\sin\frac{\pi k}{4} + \sin\frac{3\pi k}{4} + 2\sin\frac{5\pi k}{4} + 3\sin\frac{7\pi k}{4}\right)
\end{aligned} \tag{2.49}$$

Example 2.0.3. Let the following piece-wise constant function be given by:

$$f(\xi) := \sum_{j=1}^{4} \eta_j \chi_{A_j}(\xi), \tag{2.50}$$

where $j = 1, 2, 3, 4, 5$ and A_j=$[\xi_{j-1}, \xi_j]$, $\xi_0 = -3,\ \xi_1 = -1.5,\ \xi_2 = 0.2, \xi_3 = 1, \xi_4 = 2,$ and $\eta_j = [\eta_1, \eta_2, \eta_3, \eta_4] = [2, 1, 3, 6]$

$$f(\xi) = \begin{cases} 2, & -3 \leq \xi < -\frac{3}{2} \\ 1, & -\frac{3}{2} \leq \xi < \frac{1}{5} \\ 3, & 0.2 \leq \xi < 1 \\ 6, & 1 \leq \xi \leq 3 \end{cases} \tag{2.51}$$

Here we calculate the Fourier coefficients by:

$$\begin{aligned} \alpha_0 = \frac{1}{2a}\int_{-a}^{a} f(\xi)\mathrm{d}\xi = \frac{1}{6}\sum_{j=1}^{4} \eta_j(\xi_j - \xi_{j-1}) = \frac{1}{6}\Bigg[\bigg(2(-\frac{3}{2}+3)\bigg) + (\frac{1}{5}+\frac{3}{2})\bigg) + \\ 3(1-\frac{1}{5}) + 6(3-1)\bigg)\Bigg] = \frac{191}{60} \end{aligned} \tag{2.52}$$

and α_k, where $\omega = \frac{\pi}{3}$:

$$\begin{aligned} \alpha_k^j &= \frac{2\eta_j}{\pi k}\sin\left(\omega k\frac{h_j}{2}\right)\cos\left(\omega k\frac{\xi_j+\xi_{j-1}}{2}\right) \\ \alpha_k^1 &= \frac{2\cdot 2}{\pi k}\sin\left(\frac{\pi}{3}k\frac{3}{4}\right)\cos\left(\frac{\pi}{3}k\frac{9}{4}\right) = \frac{4}{\pi k}\sin\left(\frac{\pi k}{4}\right)\cos\left(\frac{3\pi k}{4}\right) \\ \alpha_k^2 &= \frac{2\cdot 1}{\pi k}\sin\left(\frac{\pi}{3}k\frac{17}{20}\right)\cos\left(\frac{\pi}{3}k\frac{13}{20}\right) = \frac{2}{\pi k}\sin\left(\frac{17\pi k}{60}\right)\cos\left(\frac{13\pi k}{60}\right) \\ \alpha_k^3 &= \frac{2\cdot 3}{\pi k}\sin\left(\frac{\pi}{3}k\frac{4}{10}\right)\cos\left(\frac{\pi}{3}k\frac{6}{10}\right) = \frac{6}{\pi k}\sin\left(\frac{2\pi k}{15}\right)\cos\left(\frac{\pi k}{5}\right) \\ \alpha_k^4 &= \frac{2\cdot 6}{\pi k}\sin\left(\frac{\pi}{3}k\right)\cos\left(\frac{\pi}{3}k\cdot 2\right) = \frac{12}{\pi k}\sin\left(\frac{\pi k}{3}\right)\cos\left(\frac{2\pi k}{3}\right) \\ \alpha_k &= \sum_{j=1}^{4}\alpha_k^j = -\frac{1}{\pi k}\left(2\sin\frac{k\pi}{15} + 3\sin\frac{k\pi}{3} + \sin\frac{k\pi}{2}\right) \end{aligned} \tag{2.53}$$

and, β_k, with $\omega = \frac{\pi}{3}$

$$
\begin{aligned}
\beta_k^j &= \frac{2\eta_j}{\pi k}\sin\left(\omega k\frac{h_j}{2}\right)\sin\left(\omega k\frac{\xi_j+\xi_{j-1}}{2}\right)\\
\beta_k^1 &= \frac{2\cdot 2}{\pi k}\sin\left(\frac{\pi}{3}k\frac{3}{4}\right)\sin\left(\frac{\pi}{3}k\frac{9}{4}\right) = \frac{4}{\pi k}\sin\left(\frac{\pi k}{4}\right)\sin\left(\frac{3\pi k}{4}\right)\\
\beta_k^2 &= \frac{2\cdot 1}{\pi k}\sin\left(\frac{\pi}{3}k\frac{17}{20}\right)\sin\left(\frac{\pi}{3}k\frac{13}{20}\right) = \frac{2}{\pi k}\sin\left(\frac{17\pi k}{60}\right)\sin\left(\frac{13\pi k}{60}\right)\\
\beta_k^3 &= \frac{2\cdot 3}{\pi k}\sin\left(\frac{\pi}{3}k\frac{4}{10}\right)\sin\left(\frac{\pi}{3}k\frac{6}{10}\right) = \frac{6}{\pi k}\sin\left(\frac{2\pi k}{15}\right)\sin\left(\frac{\pi k}{5}\right)\\
\beta_k^4 &= \frac{2\cdot 6}{\pi k}\sin\left(\frac{\pi}{3}k\right)\sin\left(\frac{\pi}{3}k\cdot 2\right) = \frac{12}{\pi k}\sin\left(\frac{\pi k}{3}\right)\sin\left(\frac{2\pi k}{3}\right)\\
\beta_k &= \sum_{j=1}^{4}\beta_k^j = \frac{1}{\pi k}\left(4\cos\frac{k\pi}{15}+3\cos\frac{k\pi}{3}+\cos\frac{k\pi}{2}-8(-1)^k\right)
\end{aligned}
\tag{2.54}
$$

3 ODE analysis: The nonlinear Schrödinger equation

In section 1.1, we have described a series of PDEs, particularly the NLSE, which is commonly used to simulate rogue waves. The time-dependent form of the NLSE for $u(x,t)$ can be represented by:

$$-\frac{1}{2}u_{xx} + \kappa|u|^2 u = iu_t \tag{3.1}$$

which we aim to study in its stationary form:

$$-\frac{1}{2}u_{xx} + \kappa|u|^2 u = 0 \tag{3.2}$$

where $\kappa = 1$ for simplicity, and where $u(x)$ is the time-*in*dependent Fourier series (which are regularized time-independent piece-wise constant functions in $\mathscr{Q}$, which has the same vector space properties as $\mathscr{S}$ however having the position variable, x). In order to obtain these time-independent functions $u(x) \in \mathscr{Q}$ for the one-dimensional problem in (3.2) we do the following.

1) The time-series in 7.2 are used to obtain a set of coordinates ($\mathcal{S}$) from approximately 100 seconds before and after the rogue wave following definition 2.1. The coordinates of the amplitudes of the waves in the wave-train are extracted in the mathematical software (i.e. Mathematica).

2) With the obtained ($\mathcal{S}$) time-series coordinates, we can either use these are direct input to generate a piecewise-constant function or we can *scale* these by multiplying the time coordinate (seconds) by the known wave-velocity (meter/seconds - see 7.2) and obtain a new set of position-dependent coordinates ($\mathcal{Q}$) and then generate a piecewise constant function.

3) Using ($\mathcal{Q}$) we generate the time-independent piece-wise constant functions $u(x)$ regularized as Fourier series which are elements of $\mathscr{Q}$.

4) The Fourier series in $\mathscr{Q}$ are finally evaluated as weak solutions to (3.2) to generate the force functions, h (which we assume to be individual for each rogue wave event). We

do this by thus considering the time-independent Fourier series of piece-wise constant function in $\mathscr{Q}$ as functions for the NLS operator

$$P := -\frac{1}{2}\frac{d^2}{dx^2} + |u(x)|^2. \tag{3.3}$$

which gives the operator equation:

$$P\big(u(x)\big) = h(x). \tag{3.4}$$

Where, as noted, $u(x)$ is the time-independent Fourier series of the piece-wise constant functions of the rogue wave readings which considered as a weak solutions to the inhomogeneous equation (3.4) and $h(x)$ is the force function. The resulting individual force functions $h(x)$ are quantified for magnitude by using the $2-norm$ by the following definition.

Definition 3.1. Let $h(x) \in L^2$ on the arbitrary interval $[-a, a]$. We can then define the 2-norm of $h(t)$ by

$$\|h(t)\|_2 := \left(\int_a^b |h(t)|^2 dt\right)^{\frac{1}{2}} \tag{3.5}$$

The calculations for the 2-norm for the respective readings are Draupner: 2.85×10^{15}, Gorm: 3.85×10^9, Black Sea: 4.45×10^{10} and Ucluelet: 7.75×10^{13}. From this quantification, we rank the calculated norms of the rogue wave with the rogue wave height (H_{max}) and the wave-train velocity (supplied in 7.2). The ranking, shows that the most powerful rogue wave event was the Draupner wave in the North Sea, by highest norm value, highest wave velocity and highest rogue wave height H_{max}. The second highest was Ucluelet, with next highest magnitude, wave velocity and H_{max}. The third and fourth are Gorm and Black Sea rogue waves. We plot the respective NLS-force functions $h(x)$ for each rogue wave event to illustrate their relationship with one another in Figure 7.

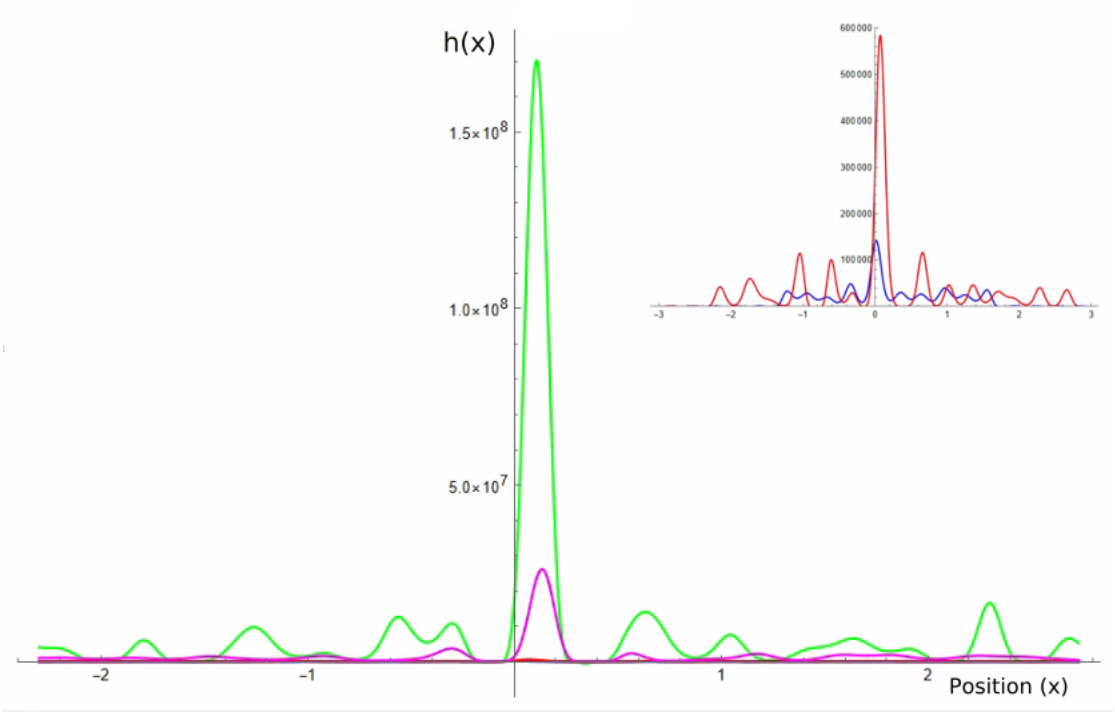

Figure 7. Force functions generated by the NLS operator for four different rogue wave events. Green: Force function of the Draupner wave (Eastern North Sea); Magenta: Force function of the Ucluelet wave (Pacific ocean); Red: Force function of the Black sea rogue wave (North-East Black sea); Blue: Force function of the Gorm rogue wave (southern North sea). x-axis: position (x), y-axis: force function $h(x)$. Inserted picture upper right: Black Sea and Gorm rogue wave force functions shown for clarity purposes.

Using the norms of the force functions, we can differentiate between the individual rogue wave to a satisfactory degree (Black Sea rogue wave was overestimated over the Gorm rogue wave). For future studies, our aim is to use several stationary functions from rogue wave readings in $\mathscr{Q}$ to develop a warning method for shipping vessels to increase their safety at sea. This work will be based on the hypothesis that a warning signal for a rogue wave is detectable in the profile of stationary force functions given in $h(x)$.

4 Conclusions

In this study, we have prepared the theoretical foundation to analyse a set of rogue wave readings from laser from oil-platforms and buoys in the ocean. This analysis is based on developing regularized functions (Fourier series) of the piece-wise constant functions of laser readings. We studied briefly the time-independent regularized functions by using them as weak solutions to the homogeneous Nonlinear Schrödinger equation and thus generated a force function. Each force function was quantified by the 2-norm, and the norm was compared with H_{max} and wave-velocity of the rogue wave event. The norms are in good agreement with H_{max} and the wave-velocity, except for an overestimation of the Black Sea rogue wave compared to the Gorm rogue wave.

5 Acknowledgements

The author wishes to thank Yury Shestopalov and Rolf Källström for their critical remarks, and Högskolan i Gävle for its advanced distance education programs.

6 References

[1] Christian Kharif and Efim Pelinovsky. Physical mechanisms of the rogue wave phenomenon. *European Journal of Mechanics-B/Fluids*, 22(6):603–634, 2003.

[2] Sergio Manzetti. Mathematical modeling of rogue waves: A survey of recent and emerging mathematical methods and solutions. *Axioms*, 7(2):42, 2018.

[3] Kristian Dysthe, Harald E Krogstad, and Peter Müller. Oceanic rogue waves. *Annu. Rev. Fluid Mech.*, 40:287–310, 2008.

[4] Wolfgang Rosenthal and Susanne Lehner. Rogue waves: Results of the maxwave project. *Journal of Offshore Mechanics and Arctic Engineering*, 130(2), 2008.

[5] Gregory A DiLisi and Richard A Rarick. Remembering the ss edmund fitzgerald. *The Physics Teacher*, 53(9):521–525, 2015.

[6] Lennart Stenflo and Mattias Marklund. Rogue waves in the atmosphere. *Journal of Plasma Physics*, 76(3-4):293–295, 2010.

[7] Nail Akhmediev, John M Dudley, Daniel R Solli, and Sergei K Turitsyn. Recent progress in investigating optical rogue waves. *Journal of optics*, 15(6):060201, 2013.

[8] Miguel Onorato, Luigi Cavaleri, Stephane Randoux, Pierre Suret, Maria Isabel Ruiz, Marta de Alfonso, and Alvise Benetazzo. Observation of a giant nonlinear wave-packet on the surface of the ocean. *Scientific Reports*, 11(1):1–7, 2021.

[9] Paul C Liu. A chronology of freaque wave encounters. *G eofizika*, 24(1):57–70, 2007.

[10] D Faulkner. An analytical assessment of the sinking of the mv derbyshire. *Journal of Ship and Ocean Technology*, 6(4):19–76, 2002.

[11] Ray Bell and Ben Kirtman. Extreme environmental forcing on the container ship ss el faro. *Journal of Operational Oceanography*, 14(2):98–113, 2021.

[12] Philip G Drazin and Robin Stanley Johnson. *Solitons: an introduction*, volume 2. Cambridge university press, 1989.

[13] Richard Courant and David Hilbert. *Methods of mathematical physics: partial differential equations*. John Wiley & Sons, 2008.

[14] Sergei Lvovich Sobolev. *Partial Differential Equations of Mathematical Physics: International Series of Monographs in Pure and Applied Mathematics*. Elsevier, 2016.

[15] Sergio Manzetti and Alexander Trounev. Modeling quantum fractals by a nonlinear quantum diffusion equation. *Technical Reports*, 2021.

[16] Vladimir Evgen'evich Zakharov and Alexey Borisovich Shabat. A scheme for integrating the nonlinear equations of mathematical physics by the method of the inverse scattering problem. i. *Funktsional'nyi Analiz i ego Prilozheniya*, 8(3):43–53, 1974.

[17] Gui Mu, Zhenyun Qin, and Roger Grimshaw. Dynamics of rogue waves on a multisoliton background in a vector nonlinear schrodinger equation. *SIAM Journal on Applied Mathematics*, 75(1):1–20, 2015.

[18] Adrian Ankiewicz and Nail Akhmediev. Rogue wave-type solutions of the mkdv equation and their relation to known nlse rogue wave solutions. *Nonlinear Dynamics*, 91(3):1931–1938, 2018.

[19] Adrian Ankiewicz, Yan Wang, Stefan Wabnitz, and Nail Akhmediev. Extended nonlinear schrödinger equation with higher-order odd and even terms and its rogue wave solutions. *Physical Review E*, 89(1):012907, 2014.

[20] Vladimir B Matveev, Mikhail A Salle, et al. *Darboux transformations and solitons*, volume 17. Springer, 1991.

[21] Chao-Qing Dai, Yue-Yue Wang, Qing Tian, and Jie-Fang Zhang. The management and containment of self-similar rogue waves in the inhomogeneous nonlinear schrödinger equation. *Annals of Physics*, 327(2):512–521, 2012.

[22] Kristian B Dysthe. Note on a modification to the nonlinear schrödinger equation for application to deep water waves. *Proceedings of the Royal Society of London. A. Mathematical and Physical Sciences*, 369(1736):105–114, 1979.

[23] Bertrand Kibler, Julien Fatome, Christophe Finot, Guy Millot, Frédéric Dias, Goëry Genty, Nail Akhmediev, and John M Dudley. The peregrine soliton in nonlinear fibre optics. *Nature Physics*, 6(10):790–795, 2010.

[24] Kristian B Dysthe and Karsten Trulsen. Note on breather type solutions of the nls as models for freak-waves. *Physica Scripta*, 1999(T82):48, 1999.

[25] D Howell Peregrine. Water waves, nonlinear schrödinger equations and their solutions. *The ANZIAM Journal*, 25(1):16–43, 1983.

[26] Nail Akhmediev, Adrian Ankiewicz, and Jose M Soto-Crespo. Rogue waves and rational solutions of the nonlinear schrödinger equation. *Physical Review E*, 80(2):026601, 2009.

[27] Paul Zimmermann, Alexandre Casamayou, Nathann Cohen, Guillaume Connan, Thierry Dumont, Laurent Fousse, François Maltey, Matthias Meulien, Marc Mezzarobba, Clément Pernet, et al. *Computational mathematics with SageMath*. SIAM, 2018.

[28] Ryogo Hirota. A new form of bäcklund transformations and its relation to the inverse scattering problem. *Progress of Theoretical Physics*, 52(5):1498–1512, 1974.

[29] Yoshimasa Matsuno. Bilinear transformation method. *Mathematics in Science and Engineering*, 174, 1984.

[30] AR Osborne. Soliton physics and the periodic inverse scattering transform. *Physica D: Nonlinear Phenomena*, 86(1-2):81–89, 1995.

[31] AR Osborne. Solitons in the periodic korteweg–de vries equation, the ftheta-function representation, and the analysis of nonlinear, stochastic wave trains. *Physical Review E*, 52(1):1105, 1995.

[32] AJ Majda, DW McLaughlin, and EG1431687 Tabak. A one-dimensional model for dispersive wave turbulence. *Journal of Nonlinear Science*, 7:9–44, 1997.

[33] A Pushkarev and VE Zakharov. Quasibreathers in the mmt model. *Physica D: Nonlinear Phenomena*, 248:55–61, 2013.

[34] Vladimir Zakharov, Frédéric Dias, and Andrei Pushkarev. One-dimensional wave turbulence. *Physics Reports*, 398(1):1–65, 2004.

[35] VE Zakharov, P Guyenne, AN Pushkarev, and F Dias. Wave turbulence in one-dimensional models. *Physica D: Nonlinear Phenomena*, 152:573–619, 2001.

[36] Will Cousins and Themistoklis P Sapsis. Quantification and prediction of extreme events in a one-dimensional nonlinear dispersive wave model. *Physica D: Nonlinear Phenomena*, 280:48–58, 2014.

[37] Will Cousins and Themistoklis P Sapsis. Unsteady evolution of localized unidirectional deep-water wave groups. *Physical Review E*, 91(6):063204, 2015.

[38] Mark J Ablowitz and Ziad H Musslimani. Integrable nonlocal nonlinear schrödinger equation. *Physical review letters*, 110(6):064105, 2013.

[39] Mark J Ablowitz and Ziad H Musslimani. Inverse scattering transform for the integrable nonlocal nonlinear schrödinger equation. *Nonlinearity*, 29(3):915, 2016.

[40] Mark J Ablowitz and Ziad H Musslimani. Integrable nonlocal nonlinear equations. *Studies in Applied Mathematics*, 139(1):7–59, 2017.

[41] Luigi Cavaleri, Francesco Barbariol, Alvise Benetazzo, Luciana Bertotti, Jean-Raymond Bidlot, Peter Janssen, and Nils Wedi. The draupner wave: A fresh look and the emerging view. *Journal of Geophysical Research: Oceans*, 121(8):6061–6075, 2016.

[42] BV Divinsky, BV Levin, LI Lopatukhin, EN Pelinovsky, and AV Slyunyaev. A freak wave in the black sea: observations and simulation. In *Doklady Earth Sciences C/C of Doklady-Akademia Nauk.*, volume 395, pages 438–443. Interperiodica Publishing, 2004.

[43] Johannes Gemmrich and Leah Cicon. Generation mechanism and prediction of an observed extreme rogue wave. *Scientific Reports*, 12(1):1–10, 2022.

[44] Johannes Gemmrich, Burkhard Baschek, and Chris Garrett. Rogue waves: rare but damaging. *Seaways*, 14(1):14–16, 2013.

7 APPENDIX

7.1 Relationship between Fourier coefficients and the arbitrary interval value a.

1. Consider α_k for the indicator function:

$$\alpha_k^j = \frac{2}{\pi k} \sin\left(\frac{\pi}{a} k \frac{h_j}{2}\right) \cos\left(\frac{\pi}{a} k \frac{\xi_j + \xi_{j-1}}{2}\right) \tag{7.1}$$

Since we have for the uniform grid that $h_j = \frac{2a}{n}$ we get:

$$\alpha_k^j = \frac{2}{\pi k} \sin\left(\frac{\pi}{a} k \frac{\frac{2a}{n}}{2}\right) \cos\left(\frac{\pi}{a} k \frac{\xi_j + \xi_{j-1}}{2}\right) \tag{7.2}$$

and since $\xi_j + \xi_{j-1} = \frac{a}{C}$, such that with $h_j = h = \frac{2a}{n}$ we get $C = \frac{h_j n}{2(\xi_j + \xi_{j-1})}$ we obtain for the indicator function:

$$\alpha_k^j = \frac{2}{\pi k} \sin\left(\frac{\pi}{n} k\right) \cos\left(\frac{\pi}{2C} k\right). \tag{7.3}$$

For the piece-wise constant function, consider again the α_k coefficient for the indicator function:

$$\alpha_k^j = \frac{2}{\pi k} \sin\left(\frac{\pi}{a} k \frac{h_j}{2}\right) \cos\left(\frac{\pi}{a} k \frac{\xi_j + \xi_{j-1}}{2}\right) \tag{7.4}$$

Now let $\xi_j = -a + jh$, $j = 0, 1, \cdots, n$. Then, let $h_j = h = \frac{2a}{n}$, $\quad j = 1, 2, \cdots, n$ and $\xi_j + \xi_{j-1} = -2a + (2j-1)h$, such that we get for the cosine term:

$$\cos\frac{\pi}{a} k \frac{(\xi_j + \xi_{j-1})}{2} = \cos\left(-\pi k + (2j-1)\frac{\pi k}{n}\right) = (-1)^k \cos\left((2j-1)\frac{\pi k}{n}\right) \tag{7.5}$$

Insert for the cosine term in (7.4) and put $w_k = \frac{\pi k}{n}$, such that we obtain:

$$\alpha_k = \frac{2(-1)^k}{\pi k} \sin w_k \sum_{j=1}^{n} \eta_j \cos\big((2j-1)w_k\big); \tag{7.6}$$

Before we can show independence of α_k for the whole piece-wise constant function using this formula, we need however to take the same approach first for the β_k coefficient, and

after express the piece-wise constant function as a Fourier series.

2. Consider the β_k coefficient for the indicator function.

$$\beta_k^j = \frac{2}{\pi k} \sin\left(\frac{\pi}{a} k \frac{h_j}{2}\right) \sin\left(\frac{\pi}{a} k \frac{\xi_j + \xi_{j-1}}{2}\right), \tag{7.7}$$

Since we have for the uniform grid that $h_j = \frac{2a}{n}$ we get:

$$\beta_k^j = \frac{2}{\pi k} \sin\left(\frac{\pi}{a} k \frac{\frac{2a}{n}}{2}\right) \sin\left(\frac{\pi}{a} k \frac{\xi_j + \xi_{j-1}}{2}\right) \tag{7.8}$$

and since $\xi_j + \xi_{j-1} = \frac{a}{C}$, such that with $h_j = \frac{2a}{n}$ we get $C = \frac{h_j n}{2(\xi_j + \xi_{j-1})}$ we obtain for the indicator function:

$$\beta_k^j = \frac{2}{\pi k} \sin\left(\frac{\pi}{n} k\right) \sin\left(\frac{\pi}{2C} k\right). \tag{7.9}$$

For the piece-wise constant function, consider the β_k coefficient for the indicator function:

$$\beta_k^j = \frac{2}{\pi k} \sin\left(\frac{\pi}{a} k \frac{h_j}{2}\right) \sin\left(\frac{\pi}{a} k \frac{\xi_j + \xi_{j-1}}{2}\right) \tag{7.10}$$

Now let $\xi_j = -a + jh$, $j = 0, 1, \cdots, n$. Then, let $h_j = h = \frac{2a}{n}$, $\quad j = 1, 2, \cdots, n$ and $\xi_j + \xi_{j-1} = -2a + (2j-1)h$, such that we get for the sine term:

$$\sin \frac{\pi}{a} k \frac{(\xi_j + \xi_{j-1})}{2} = \sin\left(- \pi k + (2j-1)\frac{\pi k}{n}\right) = (-1)^k \sin\left((2j-1)\frac{\pi k}{n}\right) \tag{7.11}$$

Insert for the cosine term in (7.10) and put $w_k = \frac{\pi k}{n}$, such that we obtain:

$$\beta_k = \frac{2(-1)^k}{\pi k} \sin w_k \sum_{j=1}^{n} \eta_j \sin\big((2j-1)w_k\big); \tag{7.12}$$

7.2 Rogue wave data

Here we present the meteorological and oceanographic information of each rogue wave event. The 4 considered events belong all to the class of rogue waves occurring in shallow waters (¡200m).

7.2.1 Draupner rogue wave

The Draupner rogue wave, occurred on 1 January 1995 at 15 UTC, at the Draupner oil rig (58°11' 19.6" N, 2° 28' 21.6" E) and had a wave height H_{max}=25.6 m high. The significant wave height (H_s) was 11m, and the wave speed was estimated to be 15m/s, with North-Western winds blowing at 30m/s [41]. The wave occurred during a strong low pressure pushing cold waters from the North Atlantic towards the southern North Sea (Fig 7), generating the conditions for this extreme rogue wave event occurring at 70 meters depth. This combination of the direction of the low-pressure movement and the transition from open Atlantic ocean to closed North sea was described by the concept of 'dynamical swell' [41] where the rogue wave is formed by strong nonlinear interactions from the active part of the wind-sea spectrum given the topology of the continental land and bottom morphology.

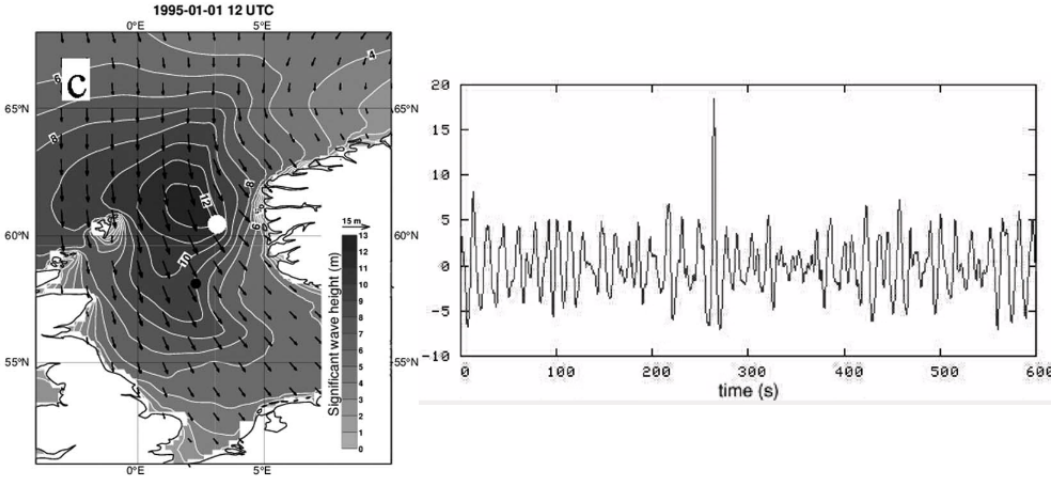

Figure 7. Draupner rogue wave event.

Left: Weather map displayed on the left with isobar scale and wind-speed indicators. White dot: location of platform. Adapted from [41] with permissions, Copyright Wiley 2016. Right: Laser-reading from the Draupner-platform. x-axis: time (sec), y-axis wave-height (m.). Adapted from [2] with permissions. Copyright MDPI Publishing 2018.

7.2.2 Gorm rogue wave

The Gorm rogue wave was recorded by the Gorm platform, in North Sea on 17 November 1984. The wind speed was 18m/s and the wave-velocity was 9m/s (by the Draupner ratio). The wind data obtained from Norwegian Meteorological Institute (https://seklima.met.no). The wave had maximal height $H_{max} = 11$ m and the significant wave height was H_s =5m [3]. The water depth at the Gorm field is 40 meters, and the rogue wave occurred in the aftermath of a North Sea storm which had its wind-speed peak on the 16th of November, 1984.

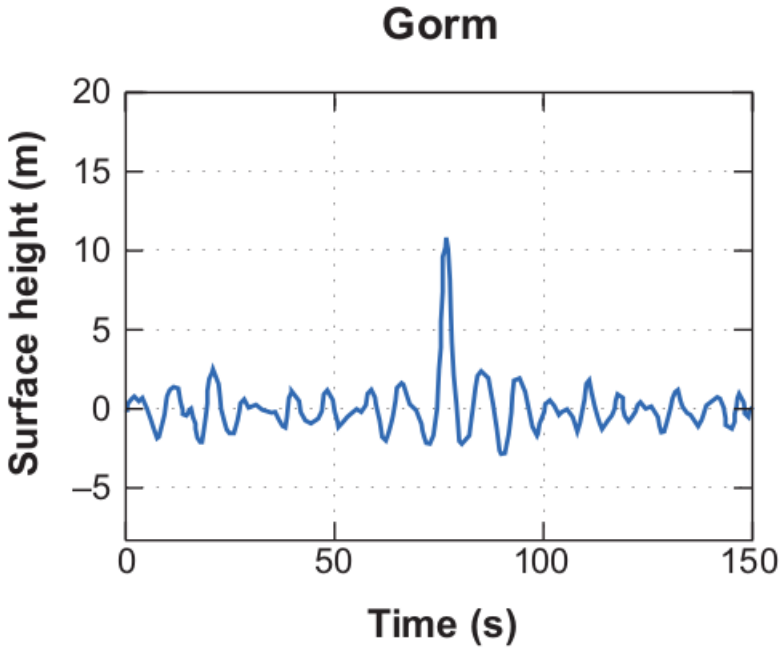

Figure 9. The Gorm rogue wave. Figure of the laser reading from the rogue wave that hit the Gorm platform outside of the Danish coast, in the North Sea. x-axis: time (sec.), y-axis: wave height (m.). Reprinted with permissions [3]. Copyright 2008 by Annual Reviews.

7.2.3 Black Sea rogue wave

The Black Sea rogue wave occurred in 1995 in the North-East sector of the Black Sea, near the city of Gelendzhik. The wave was the most steep rogue wave ever recorded on buoy readings and had a maximal height H_{max}=10.32 m (this is 3.91X times as high as the significant wave height H_s = 2.6 m). The wave had a velocity of 4.65m/s and occurred without any stormy conditions and without any registered earth quakes in the region [42].

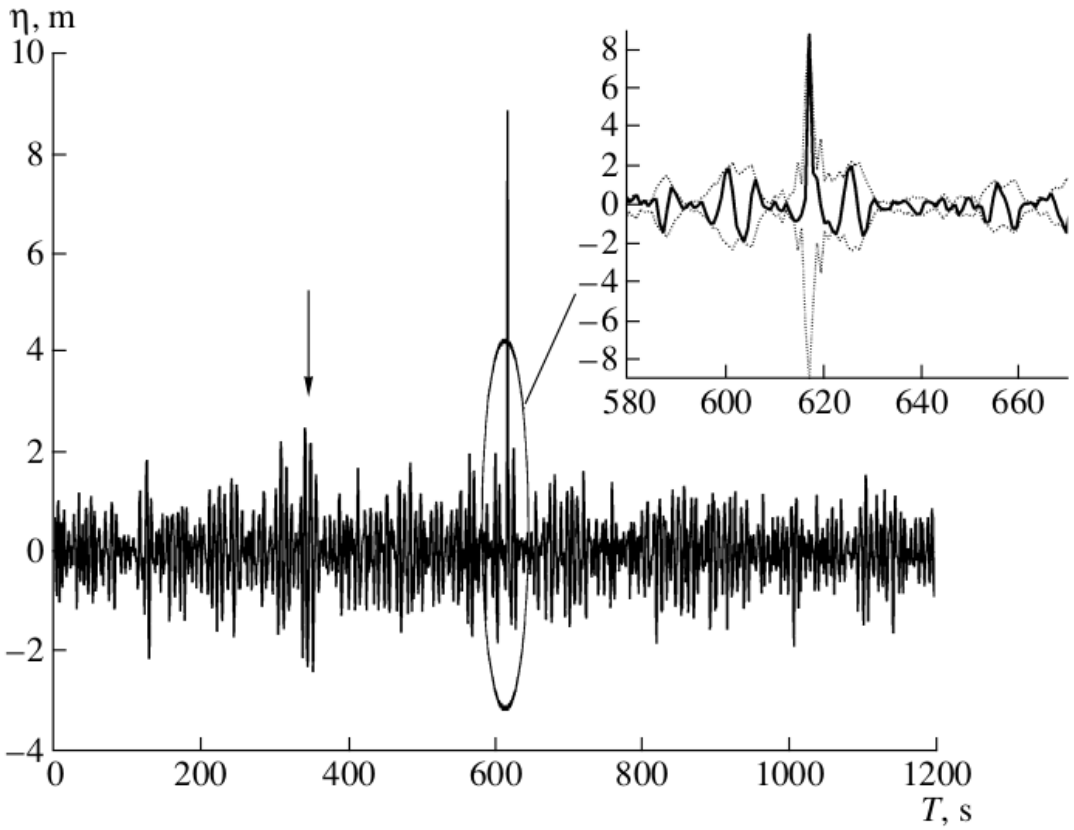

Figure 10. The Black Sea wave. Buoy reading of the Black sea rogue wave [42]. x-axis: time (sec.), y-axis: wave height (m.). Copyright 2004 by Divinsky, Levin, Lopatukhin, Pelinovsky, Slyunyaev.

7.2.4 Ucluelet rogue wave

The Ucluelet rogue wave was registered on the 17th of November 2020 by a coastal buoy stationed in the bay of Ucluelet, British Columbia [43]. The wave had a $H_{max} = 17.6$m over a standard wave height of $H_s = 6$m. The velocity of the wave was registered to and it occurred over a water depth of 45 meters, and occurred during calm weather conditions. The rogue wave speed was estimated to be 12m/s [44].

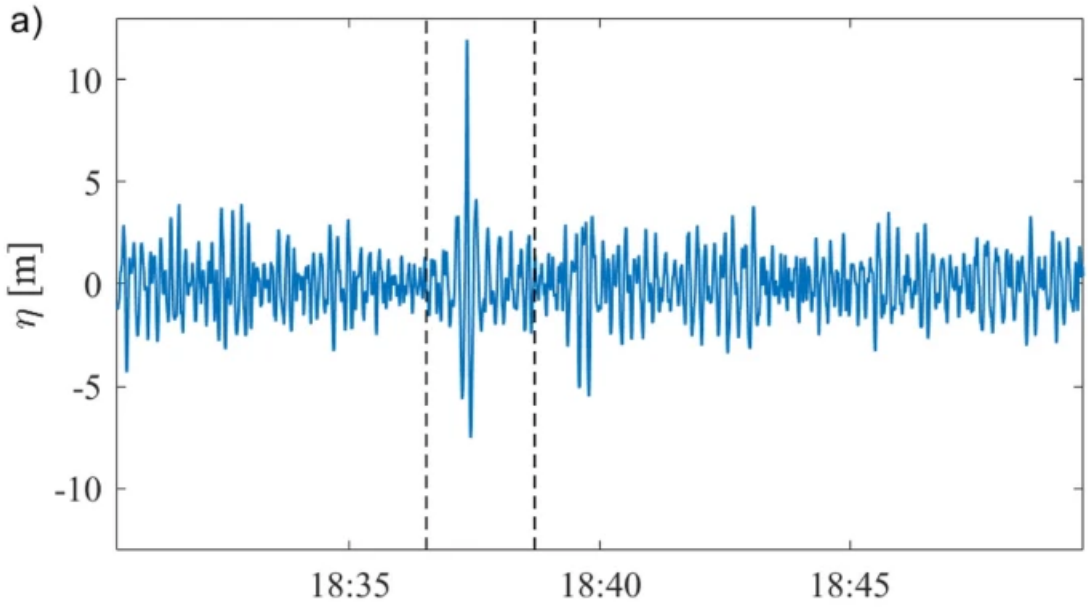

Figure 11. The Ucluelet rogue wave. Buoy reading of the rogue wave that hit the Ucluelet bay, British Columbia. x-axis: time (hrs.), y-axis wave-height (m.). Reprinted with permissions [43]. Copyright 2022 Nature publishing.

7.3 Mathematica code

University of Gaevle
Examensarbete
del II

Sergio Manzetti

Rogue wave nr. 1:
Draupner rouge wave (1994)

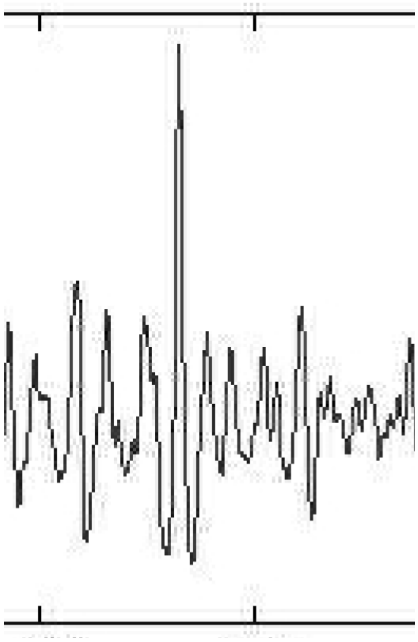

```
In[•]:= points = {{395.4416644777464`, 207.63931734339303`},
        {391.15890276860114`, 240.47382378017346`},
        {382.59337935031067`, 219.06001523444706`}, {378.3106176411653`,
         209.0669045797748`}, {369.74509422287485`, 177.65998537937617`},
        {361.1795708045843`, 250.4669344348457`}, {355.46922185905726`,
         204.78414287062958`}, {346.9036984407667`, 236.19106207102823`},
        {341.19334949523966`, 184.79792156128497`}, {332.6278260769492`,
         220.48760247082885`}, {326.9174771314222`, 214.77725352530183`},
        {322.6347154222768`, 260.4600450895181`}, {316.9243664767498`, 219.06001523444706`},
        {314.06919200398636`, 241.90141101655524`},
        {304.076081349314`, 119.12890868772422`}, {295.5105579310235`, 327.5566451994606`},
        {278.3795110944425`, 156.24617683364988`}, {269.8139876761519`, 251.8945216712275`},
        {264.1036387306249`, 196.218619452339`}, {258.39328978509786`, 286.1566153443896`},
        {249.8277663668073`, 233.33588759826466`}, {241.26224294851679`,
         173.37722367023093`}, {231.26913229384448`, 184.79792156128497`},
        {224.13119611193568`, 286.1566153443896`}, {215.56567269364515`,
         160.52893854279512`}, {199.86221309344583`, 303.28766218097076`},
        {184.1587534932465`, 72.01852988712619`}, {172.73805560219247`, 587.3775222209401`},
        {162.74494494752017`, 83.43922777818022`}, {149.89665982008435`,
         260.4600450895181`}, {145.61389811093912`, 254.74969614399106`},
        {138.47596192903032`, 317.56353454478824`}, {131.33802574712158`,
         183.37033432490318`}, {124.20008956521278`, 193.36344497957543`},
        {119.91732785606749`, 160.52893854279512`}, {112.77939167415872`,
         214.77725352530183`}, {108.49662996501345`, 199.07379392510256`},
        {105.64145549224995`, 250.4669344348457`}, {101.35869378310466`,
         324.70147072669704`}, {98.50351931034115`, 224.77036417997408`},
        {91.36558312843238`, 220.48760247082885`}, {81.37247247376007`, 96.28751290561604`},
        {75.66212352823305`, 200.50138116148423`},
        {72.80694905546954`, 351.82562821795045`}, {54.24831498250671`, 154.8185895972681`},
        {41.4000298550709`, 240.47382378017346`}, {35.68968090954388`, 236.19106207102823`},
        {32.83450643678037`, 280.4462663988626`}, {12.848285127435787`,
         131.97719381515992`}, {7.1379361819087705`, 227.62553865273765`}};
```

Shift the set of coordinates to align lowest through with the x-axis.

```
In[•]:= points2 = {⌗⟦1⟧, ⌗⟦2⟧ - 72.01852988712619`} & /@ points;
```

Generate the piecewise constant function

```
In[•]:= Clear[t];
        f[t_] = Piecewise[
           Partition[Sort[points2], 2, 1] /. {{a_?NumericQ, b_}, {c_, d_}} :> {b, a ≤ t < c}];
```

Align the rogue-wave of the piecewise constant function to the y-axis.

In[•]:=
```
f1[t_] = f[(172.73805560219247` (t + Pi) / Pi)];
Plot[f1[t], {t, -Pi, Pi}]
```

Out[•]=

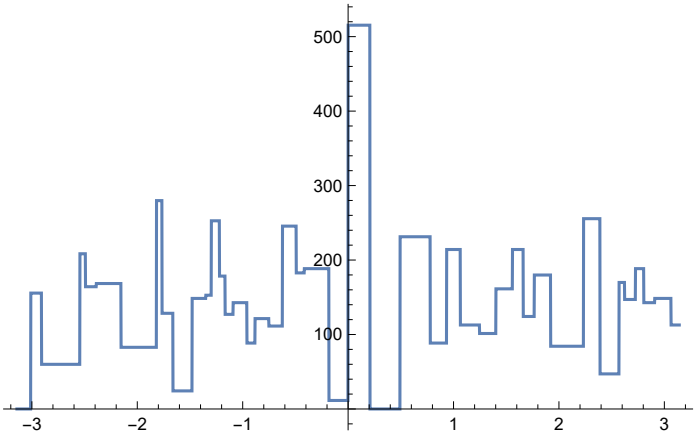

Generate Fourier series of the time-series piece-wise constant function.

In[•]:=
```
FD[t_] = FourierSeries[f1[t], t, 20]
```

Out[•]=
$$139.85 + (15.8404 + 4.76022\,i)\,e^{-i\,t} + (15.8404 - 4.76022\,i)\,e^{i\,t} + (4.64917 - 3.3024\,i)\,e^{-2\,i\,t} + (4.64917 + 3.3024\,i)\,e^{2\,i\,t} + (7.42191 - 0.300123\,i)\,e^{-3\,i\,t} + (7.42191 + 0.300123\,i)\,e^{3\,i\,t} + (0.340877 - 2.54665\,i)\,e^{-4\,i\,t} + (0.340877 + 2.54665\,i)\,e^{4\,i\,t} + (7.72422 + 6.71332\,i)\,e^{-5\,i\,t} + (7.72422 - 6.71332\,i)\,e^{5\,i\,t} + (3.16511 - 9.14479\,i)\,e^{-6\,i\,t} + (3.16511 + 9.14479\,i)\,e^{6\,i\,t} + (3.31502 + 2.18874\,i)\,e^{-7\,i\,t} + (3.31502 - 2.18874\,i)\,e^{7\,i\,t} + (9.31827 + 6.94538\,i)\,e^{-8\,i\,t} + (9.31827 - 6.94538\,i)\,e^{8\,i\,t} + (5.87173 + 18.8341\,i)\,e^{-9\,i\,t} + (5.87173 - 18.8341\,i)\,e^{9\,i\,t} + (8.75949 + 14.7107\,i)\,e^{-10\,i\,t} + (8.75949 - 14.7107\,i)\,e^{10\,i\,t} + (19.2903 + 7.78329\,i)\,e^{-11\,i\,t} + (19.2903 - 7.78329\,i)\,e^{11\,i\,t} - (3.39063 - 18.5502\,i)\,e^{-12\,i\,t} - (3.39063 + 18.5502\,i)\,e^{12\,i\,t} + (3.58427 + 18.7438\,i)\,e^{-13\,i\,t} + (3.58427 - 18.7438\,i)\,e^{13\,i\,t} + (2.66129 + 20.0781\,i)\,e^{-14\,i\,t} + (2.66129 - 20.0781\,i)\,e^{14\,i\,t} - (8.46335 - 9.96867\,i)\,e^{-15\,i\,t} - (8.46335 + 9.96867\,i)\,e^{15\,i\,t} - (8.50037 - 1.20377\,i)\,e^{-16\,i\,t} - (8.50037 + 1.20377\,i)\,e^{16\,i\,t} - (1.36102 - 16.9315\,i)\,e^{-17\,i\,t} - (1.36102 + 16.9315\,i)\,e^{17\,i\,t} - (5.78964 - 2.96094\,i)\,e^{-18\,i\,t} - (5.78964 + 2.96094\,i)\,e^{18\,i\,t} + (2.14681 + 8.29635\,i)\,e^{-19\,i\,t} + (2.14681 - 8.29635\,i)\,e^{19\,i\,t} - (3.91145 - 10.7712\,i)\,e^{-20\,i\,t} - (3.91145 + 10.7712\,i)\,e^{20\,i\,t}$$

In[•]:=
```
Plot[{FD[t]}, {t, -3, 3}, PlotRange → Full]
```

Out[•]=

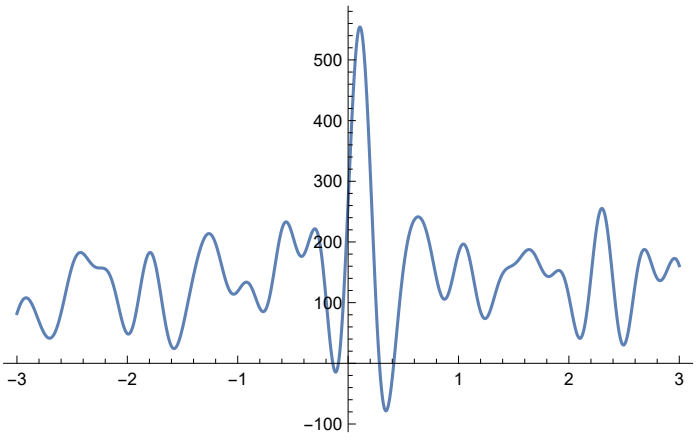

Conversion of time-series to position functions (wind-velocity: 15 meter/second).

In[ ]:=
```
pointsq = ScalingTransform[{15, 1}][points2]
```

Out[ ]=
```
{{5931.62, 135.621}, {5867.38, 168.455}, {5738.9, 147.041},
 {5674.66, 137.048}, {5546.18, 105.641}, {5417.69, 178.448},
 {5332.04, 132.766}, {5203.56, 164.173}, {5117.9, 112.779}, {4989.42, 148.469},
 {4903.76, 142.759}, {4839.52, 188.442}, {4753.87, 147.041}, {4711.04, 169.883},
 {4561.14, 47.1104}, {4432.66, 255.538}, {4175.69, 84.2276}, {4047.21, 179.876},
 {3961.55, 124.2}, {3875.9, 214.138}, {3747.42, 161.317}, {3618.93, 101.359},
 {3469.04, 112.779}, {3361.97, 214.138}, {3233.49, 88.5104}, {2997.93, 231.269},
 {2762.38, 0.}, {2591.07, 515.359}, {2441.17, 11.4207}, {2248.45, 188.442},
 {2184.21, 182.731}, {2077.14, 245.545}, {1970.07, 111.352}, {1863., 121.345},
 {1798.76, 88.5104}, {1691.69, 142.759}, {1627.45, 127.055}, {1584.62, 178.448},
 {1520.38, 252.683}, {1477.55, 152.752}, {1370.48, 148.469}, {1220.59, 24.269},
 {1134.93, 128.483}, {1092.1, 279.807}, {813.725, 82.8001}, {621., 168.455},
 {535.345, 164.173}, {492.518, 208.428}, {192.724, 59.9587}, {107.069, 155.607}}
```

Generate piece-wise constant function

In[ ]:=
```
f[x_] = Piecewise[
   Partition[Sort[pointsq], 2, 1] /. {{a_?NumericQ, b_}, {c_, d_}} :> {b, a ≤ x < c}];
```

Align the rogue wave in the piecewise constant function with the y-axis

In[ ]:=
```
f1[x_] = f[(2591.070834032887` (x + Pi) / Pi)];
Plot[f1[x], {x, -Pi, Pi}]
```

Out[ ]=

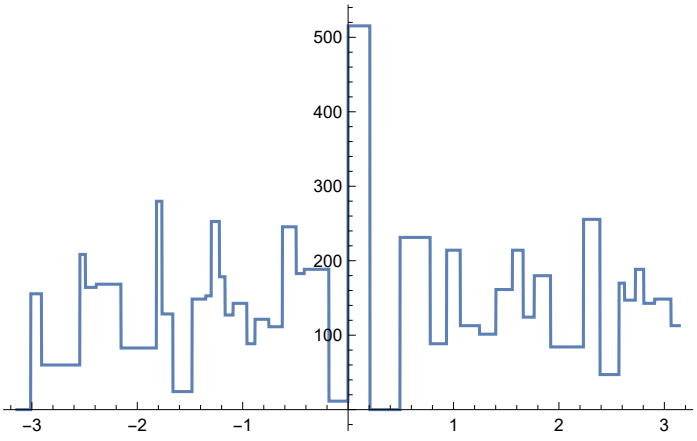

In[ ]:=
```
ud[x_] = FourierSeries[f1[x], x, 20]
```

Out[ ]=
$$\begin{aligned}
&139.85 + (15.8404 + 4.76022\,i)\,e^{-i\,x} + (15.8404 - 4.76022\,i)\,e^{i\,x} + \\
&(4.64917 - 3.3024\,i)\,e^{-2\,i\,x} + (4.64917 + 3.3024\,i)\,e^{2\,i\,x} + (7.42191 - 0.300123\,i)\,e^{-3\,i\,x} + \\
&(7.42191 + 0.300123\,i)\,e^{3\,i\,x} + (0.340877 - 2.54665\,i)\,e^{-4\,i\,x} + \\
&(0.340877 + 2.54665\,i)\,e^{4\,i\,x} + (7.72422 + 6.71332\,i)\,e^{-5\,i\,x} + (7.72422 - 6.71332\,i)\,e^{5\,i\,x} + \\
&(3.16511 - 9.14479\,i)\,e^{-6\,i\,x} + (3.16511 + 9.14479\,i)\,e^{6\,i\,x} + (3.31502 + 2.18874\,i)\,e^{-7\,i\,x} + \\
&(3.31502 - 2.18874\,i)\,e^{7\,i\,x} + (9.31827 + 6.94538\,i)\,e^{-8\,i\,x} + (9.31827 - 6.94538\,i)\,e^{8\,i\,x} + \\
&(5.87173 + 18.8341\,i)\,e^{-9\,i\,x} + (5.87173 - 18.8341\,i)\,e^{9\,i\,x} + (8.75949 + 14.7107\,i)\,e^{-10\,i\,x} + \\
&(8.75949 - 14.7107\,i)\,e^{10\,i\,x} + (19.2903 + 7.78329\,i)\,e^{-11\,i\,x} + (19.2903 - 7.78329\,i)\,e^{11\,i\,x} - \\
&(3.39063 - 18.5502\,i)\,e^{-12\,i\,x} - (3.39063 + 18.5502\,i)\,e^{12\,i\,x} + (3.58427 + 18.7438\,i)\,e^{-13\,i\,x} + \\
&(3.58427 - 18.7438\,i)\,e^{13\,i\,x} + (2.66129 + 20.0781\,i)\,e^{-14\,i\,x} + (2.66129 - 20.0781\,i)\,e^{14\,i\,x} - \\
&(8.46335 - 9.96867\,i)\,e^{-15\,i\,x} - (8.46335 + 9.96867\,i)\,e^{15\,i\,x} - (8.50037 - 1.20377\,i)\,e^{-16\,i\,x} - \\
&(8.50037 + 1.20377\,i)\,e^{16\,i\,x} - (1.36102 - 16.9315\,i)\,e^{-17\,i\,x} - (1.36102 + 16.9315\,i)\,e^{17\,i\,x} - \\
&(5.78964 - 2.96094\,i)\,e^{-18\,i\,x} - (5.78964 + 2.96094\,i)\,e^{18\,i\,x} + (2.14681 + 8.29635\,i)\,e^{-19\,i\,x} + \\
&(2.14681 - 8.29635\,i)\,e^{19\,i\,x} - (3.91145 - 10.7712\,i)\,e^{-20\,i\,x} - (3.91145 + 10.7712\,i)\,e^{20\,i\,x}
\end{aligned}$$

In[ ]:=
```
Plot[{ud[x]}, {x, -3, 3}, PlotRange → Full]
```

Out[ ]=

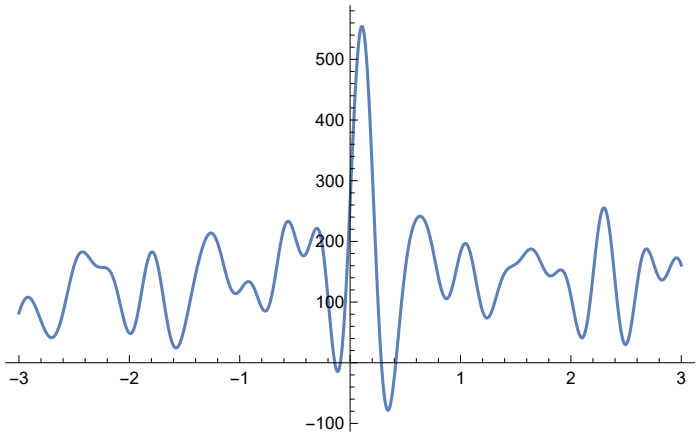

Declare the derivative for the nonlinear Schrodinger equation

In[ ]:=
```
d2U[x_] = D[ud[x], {x, 2}];
```

In[ ]:=
```
a = -3;
b = 3;
```

Generate the force function, its norm and plot by the NON LINEAR SCHRODINGER EQUATION

In[ ]:=
```
h[x_] = h[x_] = -1 / 2 * dU[x] + (Abs[ud[x]]) ^ 2 * ud[x]
NIntegrate[Abs[h[x]]^2, {x, a, b}]
Plot[h[x], {x, a, b}, PlotRange → Full]
```

Out[•]=
$$\frac{1}{2}\Big(\big(-4.76022+15.8404\,i\big)\,e^{-i\,x}-\big(4.76022+15.8404\,i\big)\,e^{i\,x}+\big(6.60479+9.29833\,i\big)\,e^{-2\,i\,x}+\big(6.60479-9.29833\,i\big)\,e^{2\,i\,x}+\big(0.900369+22.2657\,i\big)\,e^{-3\,i\,x}+\big(0.900369-22.2657\,i\big)\,e^{3\,i\,x}+\big(10.1866+1.36351\,i\big)\,e^{-4\,i\,x}+\big(10.1866-1.36351\,i\big)\,e^{4\,i\,x}-\big(33.5666-38.6211\,i\big)\,e^{-5\,i\,x}-\big(33.5666+38.6211\,i\big)\,e^{5\,i\,x}+\big(54.8687+18.9907\,i\big)\,e^{-6\,i\,x}+\big(54.8687-18.9907\,i\big)\,e^{6\,i\,x}-\big(15.3212-23.2052\,i\big)\,e^{-7\,i\,x}-\big(15.3212+23.2052\,i\big)\,e^{7\,i\,x}-\big(55.5631-74.5462\,i\big)\,e^{-8\,i\,x}-\big(55.5631+74.5462\,i\big)\,e^{8\,i\,x}-\big(169.507-52.8456\,i\big)\,e^{-9\,i\,x}-\big(169.507+52.8456\,i\big)\,e^{9\,i\,x}-\big(147.107-87.5949\,i\big)\,e^{-10\,i\,x}-\big(147.107+87.5949\,i\big)\,e^{10\,i\,x}-\big(85.6162-212.194\,i\big)\,e^{-11\,i\,x}-\big(85.6162+212.194\,i\big)\,e^{11\,i\,x}-\big(222.602+40.6875\,i\big)\,e^{-12\,i\,x}-\big(222.602-40.6875\,i\big)\,e^{12\,i\,x}-\big(243.669-46.5955\,i\big)\,e^{-13\,i\,x}-\big(243.669+46.5955\,i\big)\,e^{13\,i\,x}-\big(281.093-37.2581\,i\big)\,e^{-14\,i\,x}-\big(281.093+37.2581\,i\big)\,e^{14\,i\,x}-\big(149.53+126.95\,i\big)\,e^{-15\,i\,x}-\big(149.53-126.95\,i\big)\,e^{15\,i\,x}-\big(19.2604+136.006\,i\big)\,e^{-16\,i\,x}-\big(19.2604-136.006\,i\big)\,e^{16\,i\,x}-\big(287.835+23.1373\,i\big)\,e^{-17\,i\,x}-\big(287.835-23.1373\,i\big)\,e^{17\,i\,x}-\big(53.2969+104.214\,i\big)\,e^{-18\,i\,x}-\big(53.2969-104.214\,i\big)\,e^{18\,i\,x}-\big(157.631-40.7895\,i\big)\,e^{-19\,i\,x}-\big(157.631+40.7895\,i\big)\,e^{19\,i\,x}-\big(215.425+78.2289\,i\big)\,e^{-20\,i\,x}-\big(215.425-78.2289\,i\big)\,e^{20\,i\,x}\Big)+\Big(139.85+\big(15.8404+4.76022\,i\big)\,e^{-i\,x}+\big(15.8404-4.76022\,i\big)\,e^{i\,x}+\big(4.64917-3.3024\,i\big)\,e^{-2\,i\,x}+\big(4.64917+3.3024\,i\big)\,e^{2\,i\,x}+\big(7.42191-0.300123\,i\big)\,e^{-3\,i\,x}+\big(7.42191+0.300123\,i\big)\,e^{3\,i\,x}+\big(0.340877-2.54665\,i\big)\,e^{-4\,i\,x}+\big(0.340877+2.54665\,i\big)\,e^{4\,i\,x}+\big(7.72422+6.71332\,i\big)\,e^{-5\,i\,x}+\big(7.72422-6.71332\,i\big)\,e^{5\,i\,x}+\big(3.16511-9.14479\,i\big)\,e^{-6\,i\,x}+\big(3.16511+9.14479\,i\big)\,e^{6\,i\,x}+\big(3.31502+2.18874\,i\big)\,e^{-7\,i\,x}+\big(3.31502-2.18874\,i\big)\,e^{7\,i\,x}+\big(9.31827+6.94538\,i\big)\,e^{-8\,i\,x}+\big(9.31827-6.94538\,i\big)\,e^{8\,i\,x}+\big(5.87173+18.8341\,i\big)\,e^{-9\,i\,x}+\big(5.87173-18.8341\,i\big)\,e^{9\,i\,x}+\big(8.75949+14.7107\,i\big)\,e^{-10\,i\,x}+\big(8.75949-14.7107\,i\big)\,e^{10\,i\,x}+\big(19.2903+7.78329\,i\big)\,e^{-11\,i\,x}+\big(19.2903-7.78329\,i\big)\,e^{11\,i\,x}-\big(3.39063-18.5502\,i\big)\,e^{-12\,i\,x}-\big(3.39063+18.5502\,i\big)\,e^{12\,i\,x}+\big(3.58427+18.7438\,i\big)\,e^{-13\,i\,x}+\big(3.58427-18.7438\,i\big)\,e^{13\,i\,x}+\big(2.66129+20.0781\,i\big)\,e^{-14\,i\,x}+\big(2.66129-20.0781\,i\big)\,e^{14\,i\,x}-\big(8.46335-9.96867\,i\big)\,e^{-15\,i\,x}-\big(8.46335+9.96867\,i\big)\,e^{15\,i\,x}-\big(8.50037+1.20377\,i\big)\,e^{-16\,i\,x}-\big(8.50037-1.20377\,i\big)\,e^{16\,i\,x}-\big(1.36102+16.9315\,i\big)\,e^{-17\,i\,x}-\big(1.36102-16.9315\,i\big)\,e^{17\,i\,x}-\big(5.78964+2.96094\,i\big)\,e^{-18\,i\,x}-\big(5.78964-2.96094\,i\big)\,e^{18\,i\,x}+\big(2.14681+8.29635\,i\big)\,e^{-19\,i\,x}+\big(2.14681-8.29635\,i\big)\,e^{19\,i\,x}-\big(3.91145-10.7712\,i\big)\,e^{-20\,i\,x}-\big(3.91145+10.7712\,i\big)\,e^{20\,i\,x}\Big)\,\mathrm{Abs}\Big[139.85+\big(15.8404+4.76022\,i\big)\,e^{-i\,x}+\big(15.8404-4.76022\,i\big)\,e^{i\,x}+\big(4.64917-3.3024\,i\big)\,e^{-2\,i\,x}+\big(4.64917+3.3024\,i\big)\,e^{2\,i\,x}+\big(7.42191-0.300123\,i\big)\,e^{-3\,i\,x}+\big(7.42191+0.300123\,i\big)\,e^{3\,i\,x}+\big(0.340877-2.54665\,i\big)\,e^{-4\,i\,x}+\big(0.340877+2.54665\,i\big)\,e^{4\,i\,x}+\big(7.72422+6.71332\,i\big)\,e^{-5\,i\,x}+\big(7.72422-6.71332\,i\big)\,e^{5\,i\,x}+\big(3.16511-9.14479\,i\big)\,e^{-6\,i\,x}+\big(3.16511+9.14479\,i\big)\,e^{6\,i\,x}+\big(3.31502+2.18874\,i\big)\,e^{-7\,i\,x}+\big(3.31502-2.18874\,i\big)\,e^{7\,i\,x}+\big(9.31827+6.94538\,i\big)\,e^{-8\,i\,x}+\big(9.31827-6.94538\,i\big)\,e^{8\,i\,x}+\big(5.87173+18.8341\,i\big)\,e^{-9\,i\,x}+\big(5.87173-18.8341\,i\big)\,e^{9\,i\,x}+\big(8.75949+14.7107\,i\big)\,e^{-10\,i\,x}+\big(8.75949-14.7107\,i\big)\,e^{10\,i\,x}+\big(19.2903+7.78329\,i\big)\,e^{-11\,i\,x}+\big(19.2903-7.78329\,i\big)\,e^{11\,i\,x}-\big(3.39063-18.5502\,i\big)\,e^{-12\,i\,x}-\big(3.39063+18.5502\,i\big)\,e^{12\,i\,x}+\big(3.58427+18.7438\,i\big)\,e^{-13\,i\,x}+\big(3.58427-18.7438\,i\big)\,e^{13\,i\,x}+\big(2.66129+20.0781\,i\big)\,e^{-14\,i\,x}+\big(2.66129-20.0781\,i\big)\,e^{14\,i\,x}-\big(8.46335-9.96867\,i\big)\,e^{-15\,i\,x}-\big(8.46335+9.96867\,i\big)\,e^{15\,i\,x}-\big(8.50037+1.20377\,i\big)\,e^{-16\,i\,x}-\big(8.50037-1.20377\,i\big)\,e^{16\,i\,x}-\big(1.36102+16.9315\,i\big)\,e^{-17\,i\,x}-\big(1.36102-16.9315\,i\big)\,e^{17\,i\,x}-\big(5.78964+2.96094\,i\big)\,e^{-18\,i\,x}-\big(5.78964-2.96094\,i\big)\,e^{18\,i\,x}+\big(2.14681+8.29635\,i\big)\,e^{-19\,i\,x}+\big(2.14681-8.29635\,i\big)\,e^{19\,i\,x}-\big(3.91145-10.7712\,i\big)\,e^{-20\,i\,x}-\big(3.91145+10.7712\,i\big)\,e^{20\,i\,x}\Big]^2$$

Out[•]=
$$2.85644\times10^{15}$$

Out[ ]=